

## Micro-supercapacitors powered integrated system for flexible electronics

Liangzhu Zhang<sup>a</sup>, Dan Liu<sup>a, \*\*</sup>, Zhong-Shuai Wu<sup>b, c, \*\*\*</sup>, Weiwei Lei<sup>a, \*</sup>

<sup>a</sup> Institute for Frontier Materials, Deakin University, Waurn Ponds Campus, Locked Bag 20000, Victoria, 3220, Australia

<sup>b</sup> State Key Laboratory of Catalysis, Dalian Institute of Chemical Physics, Chinese Academy of Sciences, 457 Zhongshan Road, Dalian, 116023, China

<sup>c</sup> Dalian National Laboratory for Clean Energy, Dalian Institute of Chemical Physics, Chinese Academy of Sciences, 457 Zhongshan Road, Dalian, 116023, China



### ARTICLE INFO

#### Keywords:

Micro-supercapacitors  
2D nanomaterials  
Integrated systems  
Flexible electronics  
Energy storage  
Micro-devices

### ABSTRACT

Recently, the rapid progress of flexible electronics has attracted tremendous attention for the potential on revolutionizing human lives. Originally, flexible on-chip energy-storage devices, such as micro-supercapacitors (MSCs), have become the matchable microscale power source for wearable and portable electronics. Herein, latest advances of flexible planar MSCs and their integrated systems are briefly reviewed. Firstly, the fundamentals of flexible MSCs including planar and sandwich configuration of MSCs, one dimensional (1D) nanomaterials, 2D nanomaterials, and 2D nanocomposites electrode materials, different kinds of gel polymer electrolytes, fabrication technologies, and performance evaluation metrics are investigated. Secondly, MSCs powered integrated systems for flexible electronics with multifunction of photodetection, gas sensing, motion monitoring, body fluid monitoring, and lighting micro-LED are reviewed comprehensively. Finally, the challenges and opportunities for industrial manufacturing technology and practical applications of micro-supercapacitors powered integrated systems are briefly discussed.

### 1. Introduction

Electronics with the merits of flexibility and stretchability, behaving like a skin, have been fast developed and revealed the ability of significantly changing our daily life [1–5]. These technologies have already applied on wearable sensors and commercial flexible displays, such as LG organic light-emitting diode TV panel, Huawei foldable phone, and Xiaomi sports bracelet [6–10]. Therefore, there is a rapid demand of flexible energy storage devices with excellent performances of light-weight, bendability, small volume, high energy density and power density [11,12]. In order to fulfil the requirements of flexible electronics with multifunctional properties, such as health and industrial monitoring, integrating energy harvester, energy storage units, and working units together as an all-in-one system on one substrate is a general strategy [8, 13,14]. However, commercially available power sources, including thin-film batteries and electrochemical supercapacitors, are oversized for these devices [15–18].

Owing to high power density and long-life span, micro-supercapacitors (MSCs) are considered as promising on-chip energy storage units [19,20]. MSCs and traditional supercapacitors shared the

same charge storage process via fast ion absorption/desorption or quick and reversibly redox reactions. The bulky conventional supercapacitors are consisted of two current collectors and activated carbon electrodes isolated by separator in aqueous electrolyte. MSCs is defined as a kind of supercapacitor with submillimetre-scale microelectrodes and footprint area about  $1\text{ cm}^{-2}$ , which significantly reduced the volume of devices, and improved feasibility of packaging with flexible electronics [8,14,21]. Based on the energy storage mechanism, MSCs could be classified into symmetric and asymmetric categories. Symmetric MSCs commonly applied active materials with high-surface area and good conductivity as electrode materials, such as graphene and activated carbon, which store energy in efficient electrical double layer capacitor (EDLC) via fast and reversible adsorption and desorption of electrolyte ions at the activated surface (Fig. 1). Carbon based materials with abundant micropores and mesopores are highly desired for symmetric MSCs. The pores function as electrolyte reservoirs for electrolyte ions diffusion and greatly shorten ions transport length, and therefore, enhancing the specific capacitance. In addition, the heteroatom doping (B, F, P, N) on carbon matrix could hugely enhance the capacitance via generating faradaic reaction, changing the density near Fermi level to increase the quantum

\* Corresponding author.

\*\* Corresponding author.

\*\*\* Corresponding author.

E-mail addresses: [dan.liu@deakin.edu.au](mailto:dan.liu@deakin.edu.au) (D. Liu), [wuzs@dicp.ac.cn](mailto:wuzs@dicp.ac.cn) (Z.-S. Wu), [weiwei.lei@deakin.edu.au](mailto:weiwei.lei@deakin.edu.au) (W. Lei).

<https://doi.org/10.1016/j.ensm.2020.05.025>

Received 14 January 2020; Received in revised form 22 May 2020; Accepted 25 May 2020

Available online 15 July 2020

2405-8297/© 2020 Elsevier B.V. All rights reserved.

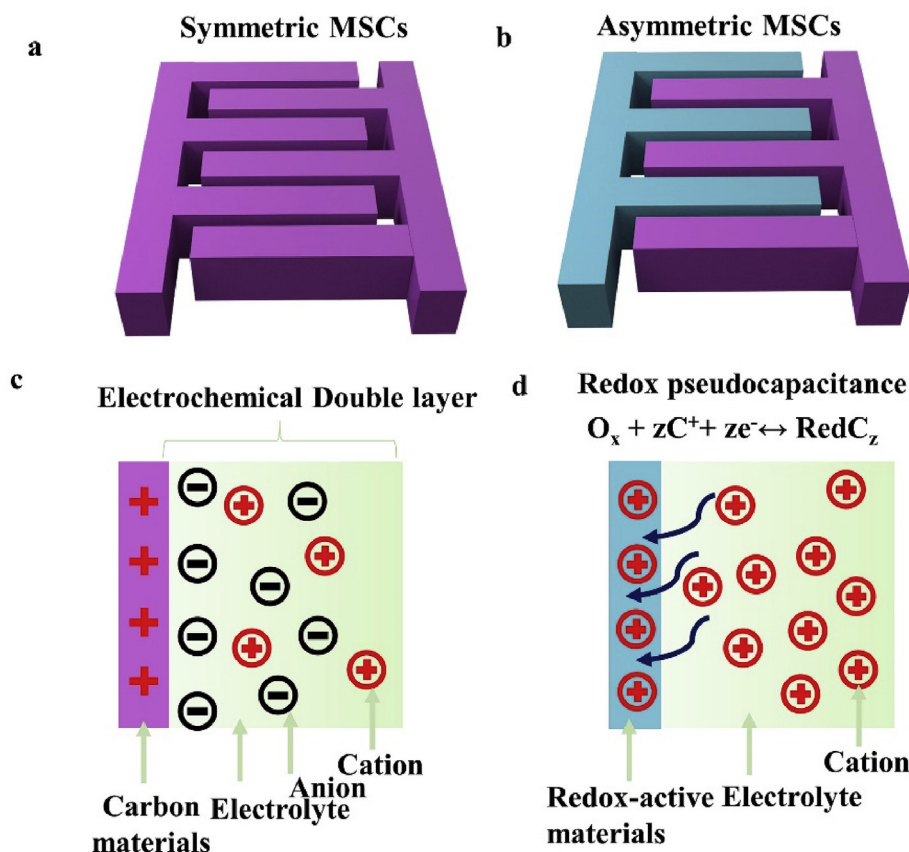


**Fig. 1.** Illustration of energy storage mechanisms of symmetric and asymmetric MSCs. (a) and (b) Schematic presentation of configuration for symmetric and asymmetric MSCs. (c) EDLC based electrodes. (d) Redox pseudocapacitive based electrodes.

capacitance, and improving the affinity to electrolyte ions [15,22–25]. For instance, F-doped graphene and B-doped graphene MSCs presented remarkable areal capacitances of  $17.4 \text{ mF cm}^{-2}$  and  $16.5 \text{ mF cm}^{-2}$  respectively, which were almost ten-fold higher compared with undoped graphene MSCs. Notably, the symmetric MSCs delivered a high power density up to  $1191 \text{ W cm}^{-3}$  [19,20,26–28]. However, their energy densities are still challenging. Therefore, pseudocapacitive nanomaterials, like MXene, conductive polymer, and transition metal oxide, have been applied for making symmetric MSCs to improve the energy storage capacity (Fig. 1) [29–35]. In addition, asymmetric MSCs with wider voltage output and larger energy density than symmetric MSCs are recently investigated [24,36–41]. Zhang et al. reported the asymmetric MSCs based on plasma reduced and nitrogen doped graphene oxide (PNG) and molybdenum dioxide delivered a wide voltage window of 1.4 V and exceptional energy density of  $38.1 \text{ mWh cm}^{-3}$  by using PVA/LiCl gel electrolyte, which is much better than energy density ( $<10 \text{ mWh cm}^{-3}$ ) and voltage window ( $<1 \text{ V}$ ) of graphene based symmetric MSCs [24]. In addition, Qin et al. fabricated the asymmetric VN//MnO<sub>2</sub> MSCs, presenting an outstanding energy density of  $21.6 \text{ mWh cm}^{-3}$  with operating window of 2 V, which greatly exceeded the energy density  $\sim 4.9 \text{ mWh cm}^{-3}$  of symmetric MnO<sub>2</sub> MSCs and energy density of  $2.2 \text{ mWh cm}^{-3}$  for symmetric VN MSCs [32]. Moreover, to further improve the energy density of MSCs, novel kinds of planar hybrid MSCs have been developed, including zinc ion micro-capacitors (ZIMCs) and lithium ion micro-capacitors (LIMCs) [42–44]. For example, LIMCs delivered a record high volumetric energy density of  $53.5 \text{ mWh cm}^{-3}$  and voltage window of 3 V for a single cell by using activated graphene as the cathode and lithium titanate nanospheres as the anode [44]. On the other hand, intensive research has been devoted to develop various fabrication methods for large-scale production of MSCs with high energy storage performance, such as micro-electro-mechanical systems (MEMS)

fabrication, screen printing, vacuum filtration, electrochemical deposition, and inkjet printing [36,37,41,45]. Considering the cost, reproducibility and scalable production possibility, screen printing, inkjet printing and vacuum filtration are frequently applied to fabricate flexible MSCs [46–53]. For instance, screen printing has been used as industrially applicable protocol for producing graphene based in-plane MSCs. The MSCs exhibited shape diversity, excellent flexibility, and modularization, which could be fabricated 130 serially-connected cells and deliver a high voltage output 100 V [46]. The quality of MSCs by screen printings is highly relied on the ink's affinity to substrates, the viscosity of ink and strength of mesh materials. Therefore, the challenge for screen printings is preparing optimal inks which could finely diffuse through the mask without dispersing to un-patterned area [54]. Ink-jet printing is a maturely and commercially available technology which directly converts the liquid inks into solid active materials in various substrates. The challenge for ink-jet printing is turning the objective nanomaterial into optimized inks without clogging nozzle when printing electrodes for MSCs [55]. For instance, jet machine was applied on direct printing MSCs by using additive-free MXene inks, which offers a promising way for low-cost and scalable production of flexible electronics with a high degree of geometry flexibility [50]. The fine-printed patterns achieved high resolution of  $120 \mu\text{m}$  and spatial uniformity within  $\sim 5.6\%$ . Moreover, the obtained MXene MSCs exhibited an ultra-high volumetric capacitance of  $562 \text{ F cm}^{-3}$ , outperforming all other printed MSCs. Vacuum filtration is a lab scale technology which is efficient and facile for preparing 2D based nanomaterials to form layer films electrodes on various substrates or freestanding electrodes. Key requirement for vacuum filtration is the stable and good dispersibility of colloid 2D solution or dispersion to form the homogenous and high-quality films [56]. Vacuum filtration was applied to fabricate highly stretchable MSCs. For example, by taking graphene, carbon nanotube (CNT), and poly (3,

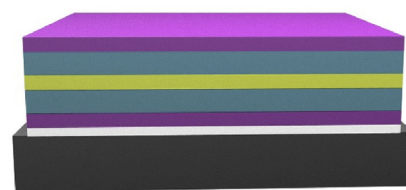
4-ethylenedioxythiophene):poly-(4-styrenesulfonate) (PEDOT:PSS) as electrode materials and rubber as substrate, the micro-device can stretch 200% and excellent capacitance retention ability after 8000 cycles under repeatedly stretch-and-release strain test [57].

Considering the above, the MSCs as a promising in-plane energy storage unit for flexible electronics are only produced in lab scale and their applications on integrated system for practical sensing or detecting are still in infancy [58–62]. In light of this, we reviewed the recent advances of fabrication techniques for high-performance flexible MSCs and MSCs based integrated systems as a novel flexible electronics prototype for body and environmental monitoring. In details, fundamentals, such as storage mechanisms and key parameters for evaluating the performance of MSCs, were summarized. The requirements of electrolyte and electrode materials for flexible MSCs were investigated. Cost-effective fabrication methods for flexible MSCs were discussed. Furthermore, MSCs based integrated systems, including power generator and multi-functional sensor, are surveyed to exhibit promising applications for flexible electronics.

## 2. Fundamentals of flexible micro-supercapacitors

### 2.1. Design

There are different shapes of micro-supercapacitors, but the basic design has two types: sandwich and in-plane configuration as demonstrated in Fig. 2 [8]. As a basic energy storage unit, the components of MSCs are electrode materials, ionic conductive electrolyte, substrate, and current collector. Inspiring by the structure of cell batteries, the first solid state thin film MSCs was invented with a sandwich structure of RuO<sub>2</sub>/lithium phosphorus oxynitride (LiPON)/RuO<sub>2</sub>/Pt (Fig. 3), in which RuO<sub>2</sub> served as electrode material and glassy solid state LiPON as electrolyte [63]. The sandwich structure is a standard configuration for industrial and efficient fabricating thin-film batteries [64,65]. However, for flexible electronics applications, the initial designed MSCs suffered from low specific capacitance and poor flexibility due to the brittle and low conductivity (<5 μS cm<sup>-1</sup>) of LiPON [63]. Sandwich type MSCs with separator remains challenging to precise control both the thickness of the separator and electrodes, which have a great impact on the degradation of specific capacity [66–68]. On the other hand, MSCs have another type of structure with microelectrodes interdigital arranged the same plane (Fig. 2b). The in-plane design is electronically isolated by physical separation with more advantages in flexibility, fabrication and reliability without using the separator [69]. The first in-plane MSCs based on conducting polymer which contained 50 paralleled microelectrodes with a short gap of 50 μm was fabricated by microelectromechanical system (MEMS) technology [70]. The specific capacitance and voltage output of this devices could be tuned by designing different patterns. As the in-plane MSCs have a narrow gap which shortened the ions diffusion paths, it decreases the charge/discharge time resulting in a higher power capacity. In addition, the thickness of electrode is below 10 μm, which is negligible compared with the thickness of substrate. Furthermore, the



■ Si substrate ■ TiO<sub>2</sub> ■ RuO<sub>2</sub> ■ LiPON ■ LiPON

Fig. 3. The structure of RuO<sub>2</sub>/Li<sub>2,94</sub>PO<sub>2,37</sub>N<sub>0,75</sub>(LiPON)/RuO<sub>2</sub>/Pt solid-state thin-film supercapacitor.

microelectrodes could be directly patterned on the targeted flexible substrates. All these advantages make the in-plane MSCs an attractive micro-scale energy storage unit for powering flexible electronics.

### 2.2. Electrode materials for flexible MSCs

Flexible MSCs as an ultra-fast and rechargeable electrochemical energy storage unit require electrode materials with excellent mechanical properties, lightweight, compacted design, and outstanding electrochemical properties. The in-plane design demands all components integrated on the same plane, which can facilitate and smooth the ions transport when MSCs work under mechanical strain [56]. Plenty of studies have been focused on reducing the thickness of electrode to improve the flexibility and capacitance retention ability under different bending states for MSCs [71–74]. According to the previous reports, electrode materials for MSCs were classified as 1D nanomaterials, 2D nanomaterials, and 2D nanocomposites [12,13].

1D nanomaterials were exploited to form nanofibers by strong entangling with each other [75,76]. CNT as a traditional 1D material was used to fabricate flexible CNT-rGO fibres, as illustrated in Fig. 4a [77]. The mixture of acid-functionalised single walled CNT (SWNT), GO and ethylenediamine (EDA) was pumped into a flexible silica tube and subjected to heat treatment at 220 °C for 6 h, and washed in water. The obtained CNT-rGO fibre was flexible and could be rolled into ring shape (Fig. 4b). Fig. 4c and d presented the parallelly connected MSCs based on the CNT-rGO fibre. The output current of the parallel MSC was lineally correlated with the numbers of MSCs. The discharge time of three parallel MSCs was three times higher than that of a single MSC. The MSCs delivered an ultra-high volumetric capacity of 300 F cm<sup>-3</sup> in polyvinyl alcohol (PVA)/H<sub>3</sub>PO<sub>4</sub> electrolyte. The volumetric energy density of 6.3 mWh cm<sup>-3</sup> was tenfold higher than that of commercially available supercapacitors. Furthermore, the MSCs presented ultra-long cycling stability after 10,000 cycles and excellent flexibility under 90° bending [77]. Jiang et al. reported MSCs produced by multi-walled CNT and nitrogen doped reduced graphene oxide (RGO) hybrid fibres (MWCNT-RGO) through hydrothermal treated in a space confinement fillers (Fig. 4e) [78]. The obtained MWCNT-RGO fibres diameters could be tuned by using the reactors with different size channels and diameters (Fig. 4g). The output voltage of the serially connected MWCNT-RGO

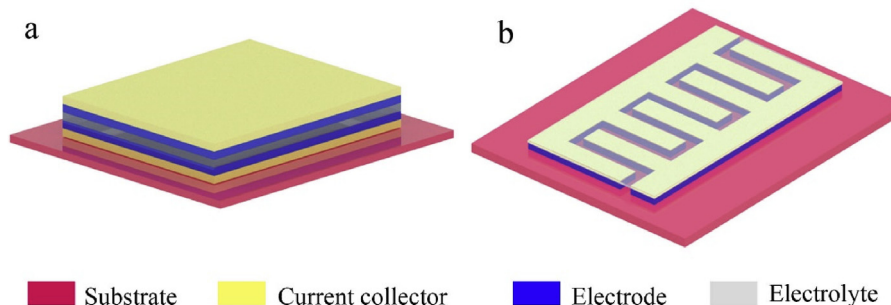
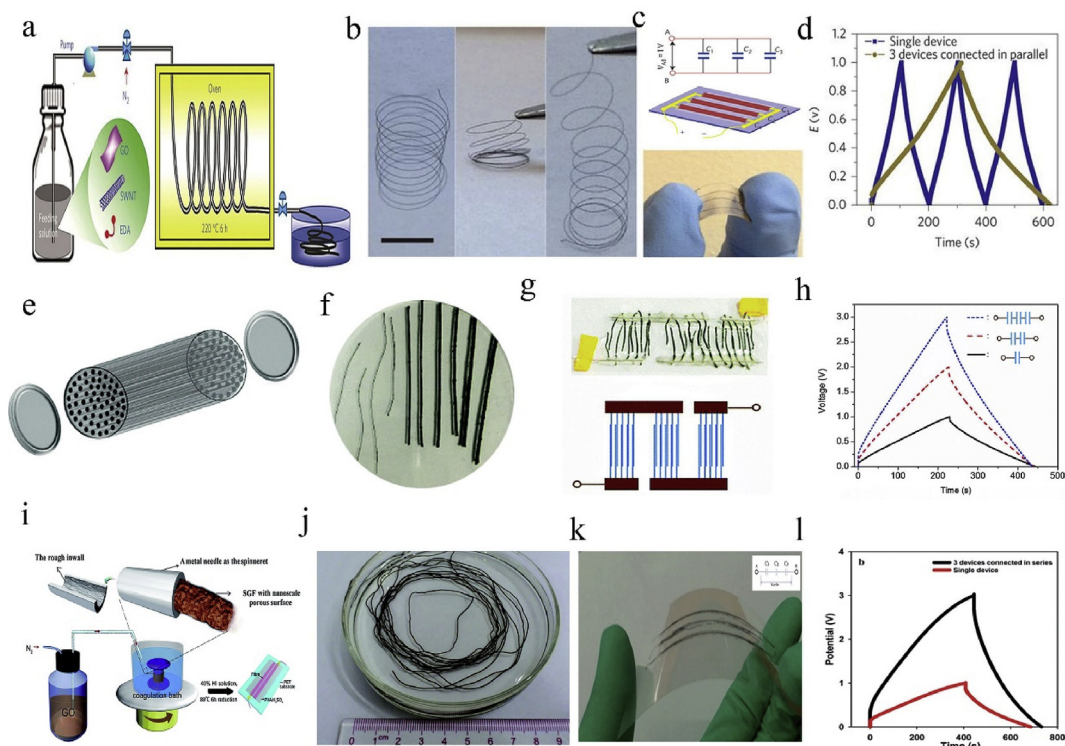


Fig. 2. Schematics of configuration of MSCs. (a) Sandwich type. (b) In-plane type.



**Fig. 4.** (a) Schematic process of fabricating CNT-rGO microfibrils. (b) Compressed and stretched fibre springs. (c) Equivalent circuit and photo of three parallelly connected CNT-rGO MSCs. (d) GCD profiles of single and three parallelly connected CNT-rGO MSCs. Reproduced with permission from Ref. [77]. Copyright 2014 Springer Nature. (e) Schematic illustration of hydrothermal reactors with cylindrical channels. (f) Photo of rGO/MWCNT hybrid fibres with different diameters. (g) Equivalent circuit and photo of three serially connected rGO/MWCNT MSCs. (h) GCD curves of single, two, and three serially connected rGO/MWCNT MSCs. Reproduced with permission from Ref. [78]. Copyright 2016 Royal Society of Chemistry. (i) Schematic presentation of producing continuously neat graphene fibres by wet spinning. (j and k) Photos of graphene fibres and serially connected graphene MSCs. (l) GCD curves of single and serially connected graphene MSCs. Reproduced with permission from Ref. [79]. Copyright 2015 Royal Society of Chemistry.

MSCs was lineally improved with the increasing of the cell number (Fig. 4h). The nitrogen-doping effects of RGO and good electrical conductivity of  $34.5 \text{ S cm}^{-1}$  synergetically contributed to the high specific volumetric capacitances of  $281 \text{ F cm}^{-3}$  of MWCNT-RGO MSCs. Furthermore, Cai et al. reported a wet spinning method for fabricating GO fibres via syringe's metal needle (Fig. 4i) [79]. The reduced GO fibres by HI acid (SGF) exhibited excellent flexibility (Fig. 4j and k). The serially connected SGF MSCs presented linear dependence between voltage output and number of MSCs (Fig. 4l). The energy density of SGF-MSCs was  $7.9 \mu\text{Wh cm}^{-2}$ , which was comparable to those of thin-film lithium batteries.

In addition, decorating carbon fibre or copper wire with capacitive materials by hydrothermal treatment or electrodeposition was also exploited for fabricating flexible MSCs. For example, carbon fibre/ $\text{MnO}_2$  [80], carbon fibre/ $\text{NiCo}_2\text{O}_4$  [81], and copper wire/ $\text{CuO@CoFe-LDH}$  have been designed for making MSCs [82], respectively. However, the small contact area for 1D nanomaterials results in the degradation of capacitance during repeated bending tests, which is unfavourable for practical applications. Therefore, 2D nanomaterials for MSCs have attracted more attention recently due to their ultrathin structure, high specific surface areas, strong mechanical stability, and exceptional electrochemical properties.

Various 2D nanomaterials have been successfully applied as electrode materials for high-performances MSCs. Among them, graphene and MXene as prototypical 2D materials have been widely investigated [33, 39,47,50,52,83–86]. Zhang et al. developed a direct printing MSCs with various patterns based on additive-free MXene ink (Fig. 5a and Fig. 5b) [50]. The printed MXene MSCs delivered excellent volumetric capacitance of  $562 \text{ F cm}^{-3}$  and energy density of  $0.32 \mu\text{Wh cm}^{-2}$  as well as good flexibility without capacitance degradation under various bending states

(Fig. 5c). In addition, MSCs prepared by direct printing or extrusion method revealed excellent capacitance retention of 97% and 100% respectively, after 14,000 cycles. Furthermore, MXene composites MSCs were produced by a facile laser-cutting kirigami patterning process on MXene/bacterial cellulose nanocomposites paper. The resulting MSCs were stretchable and bendable with outstanding areal capacitance of  $111.5 \text{ mF cm}^{-2}$ . Kaner et al. demonstrated a general and scalable method for producing graphene based MSCs by laser scribing on graphene oxide films (LSG) via commercial LightScribe [87]. This method was also applicable on other flexible polymer substrate, such as polyethylene terephthalate (PET). These MSCs exhibited highly flexibility under various bending and twisting states without changes of structural integrity [87].

Recently, Wu et al. reported a vacuum filtration method for fabricating flexible MSCs [56,88]. 2D materials such as fluorine-doped graphene (FG), phosphorene and graphene (PG) nanosheets nanocomposites were used for MSCs (Fig. 5d–e). The FG MSCs presented excellent mechanical flexibility without capacitance deterioration under bending test (Fig. 5f) [56]. The FG MSCs delivered a ultra-high energy density of  $56 \text{ mWh cm}^{-3}$ , outperforming most reported MSCs. Moreover, Wu's group has applied screen printing strategy for scalable fabrication of flexible MSCs with various patterns, exhibiting remarkable stability (Fig. 5g–i) [46].

Although graphene based MSCs demonstrated remarkable flexibility and specific capacitance compared with commercially available supercapacitors, their energy densities are still relatively low compared with lithium thin films batteries. In order to improve the energy density, hybridising pseudocapacitive materials with graphene as a composites electrode is an efficient strategy. Pseudocapacitive nanomaterials are usually with poor electrical conductivity that hinders the electrochemical

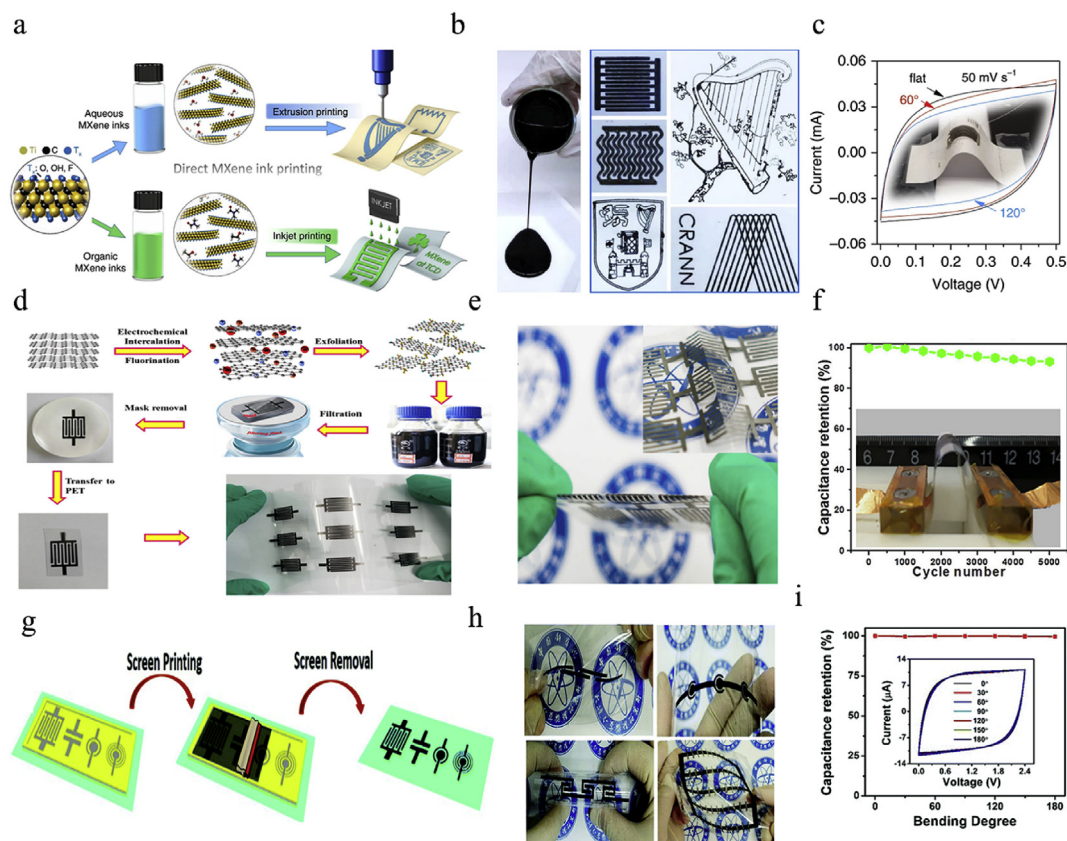


**Fig. 5.** (a) Schematic illustration of direct MXene ink printing. (b) Photographs of printed all-MXene MSCs. (c) CV curves of printed MXene MSCs under various bending degrees. Reproduced with permission from Ref. [50]. Copyright 2019 Springer Nature. (d) Schematic fabrication of FG-MSCs. Reproduced with permission from Refs. [56]. Copyright 2018 American Chemical Society. (e) Photograph of folded PG-MSCs. Reproduced with permission from Ref. [88]. Copyright 2017 American Chemical Society. (f) The CV curves under bending of FG-MSCs, the insert is the photograph of bending test. (g) Illustration of screen printing of SPG-IMSCs. (h) Photographs of SPG-IMSCs with diverse geometries. (i) Capacitance retention of SPG-IMSCs tested under different bending states. Reproduced with permission from Ref. [46]. Copyright 2019 Royal Society of Chemistry.

performance. Graphene has high conductivity that endows the nanocomposites with synergistic advantages of excellent electrochemical activity and good conductivity [39]. For instance, Wang et al. took this design idea by using liquid exfoliated graphene as conductive matrix, porous vanadium nitride (VN) and  $\text{Co}(\text{OH})_2$  nanoflowers as pseudocapacitive materials to fabricate porous VN/graphene and  $\text{Co}(\text{OH})_2$ -graphene 2D nanocomposite for planar asymmetric MSCs (Fig. 6a and b) [37]. The obtained micro-device delivered wide voltage output of 1.4 V (Fig. 6c, d and 6e), outstanding areal capacitance of  $33.4 \text{ mF cm}^{-2}$  and volumetric capacitance of  $39.7 \text{ F cm}^{-3}$  at  $0.2 \text{ mA cm}^{-2}$  (Fig. 6f).

To give a more conclusive understanding of the electrode materials for flexible in-plane MSCs, Table 1 summarized the recent advances of flexible planar MSCs based on 1D nanomaterials, 2D nanomaterials, and 2D nanocomposites. Future research should give more attention on highly conductive and pseudocapacitive 2D materials as electrode materials to fabricate high performance MSCs.

### 2.3. Electrolyte for flexible MSCs

As mentioned in the design of planar MSCs, the electrolyte covered on the surface of microelectrodes is one of the most important components for their stability, flexibility, and electrochemical performances. Advantaged electrolytes with wide voltage window, high electrochemical stability, high conductivity, low cost, and low toxicity are highly required. To date, gel polymer electrolyte is widely used due to its good mechanical strength, high stability, and high ionic conductivity around  $10^{-3} \text{ S cm}^{-1}$  [97].

Gel polymer electrolytes contain supporting polymeric framework as the matrix, liquid solvent (organic or aqueous) as the plasticizer, and

electrolytic salt. Based on types of electrolytic salt, four kinds of gel polymer electrolytes are summarized for flexible MSCs: (1) lithium ion gel polymer electrolytes, (2) proton conducting gel polymer electrolytes, (3) alkaline gel polymer electrolytes, (4) other ion gel polymer electrolytes [97].

Lithium ion gel polymer electrolytes are typically applied on Li ion batteries as well as supercapacitors. Various lithium gel polymer electrolytes, such as PVA/ $\text{LiClO}_4$ , PVA/ $\text{LiCl}$ , and polymethyl methacrylate (PMMA)/ $\text{LiClO}_4$  have been developed for flexible MSCs [37,74,91]. For instance, Geumbee et al., reported that MWNT/ $\text{Mn}_3\text{O}_4$  MSCs using an air-stable PMMA-PC- $\text{LiClO}_4$  gel electrolyte delivered a wide and stable voltage of 1.2 V [98]. Notably, the MSCs showed an excellent stability with 85% capacitance retention after 2 weeks in ambient environment without encapsulation and ultra-long life span up to 30,000 cycles with negligible capacitance degradation.

Protons with smaller ion radius than  $\text{Li}^+$  ions are promising as electrolyte salt ions for MSCs [57]. Proton conducting gel polymer electrolytes, including PVA/ $\text{H}_2\text{SO}_4$ , PVA/ $\text{H}_3\text{PO}_4$ , are commonly used for MSCs [39,56,87]. Fig. 7a and b showed the highly stretchable MSCs which is composed of graphene/CNT/cross-linked PH1000 film as electrode materials and PVA- $\text{H}_3\text{PO}_4$  as electrolyte. The excellent stretchability under strain up to 200% was evidenced from the overlapped CV and GCD curves (Fig. 7c and d). The outstanding cycling stability was also demonstrated under repeated cycling tests with 93.2% of initial capacitance remained (Fig. 7e) [57]. Recently, alkaline gel polymer electrolytes have been extensively investigated due to their wide applications in supercapacitors and rechargeable batteries. Pseudocapacitive materials, such as transition metal oxides, harvest redox reaction with  $\text{OH}^-$  ions

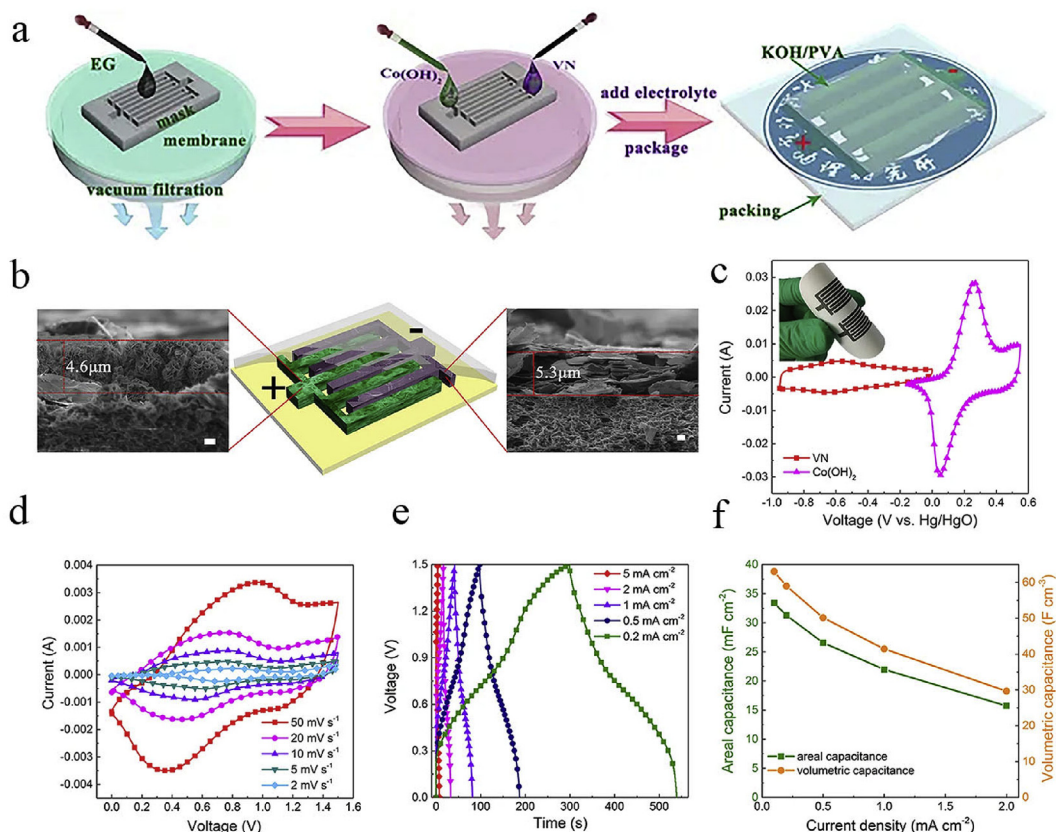


**Fig. 6.** (a) Fabrication process of VN//Co(OH)<sub>2</sub>-MSCs (b) Schematic demonstration of VN//Co(OH)<sub>2</sub>-MSCs. (c) CV curves of VN and Co(OH)<sub>2</sub> electrodes tested in a three electrode cell. (d) CV and (e) GCD curves for VN//Co(OH)<sub>2</sub>-MSCs. (f) Areal capacitance and volumetric capacitance versus current density. Reproduced with permission from Ref. [37]. Copyright 2018 Springer Nature.

which used alkaline gel polymer electrolytes for supercapacitors, such as PVA/KOH, PEO/KOH, and poly(epichlorohydrin-co-ethylene oxide) P(ECH-co-EO)/KOH [37]. As a presentative example, Wang et al. reported the fabrication of VN//Co(OH)<sub>2</sub>-AMSCs using alkaline gel electrolyte of KOH/PVA, providing excellent capacitance retention ability with only 16% loss after 10,000 cycles test [37].

On the other hand, ionic liquid electrolyte triggered lots of attentions due to its wide voltage window (approaching 4 V) and high ionic conductivity ( $>10^{-3}$  S cm<sup>-1</sup>) [99,100]. In general, ion gel polymer electrolyte is prepared by adding ionic liquid, such as ethyl-3-methylimidazolium tetrafluoroborate (EMIMBF<sub>4</sub>), into a polymer, such as potassium poly(acrylate) (PAAK) and poly(vinylidene fluoride-hexafluoropropylene) (PVDF-HFP). For instance, Zhou et al. developed a EMIMBF<sub>4</sub>/PVDF-HFP electrolyte with higher ionic conductivity of 25 mS cm<sup>-1</sup> for FG-MSCs with a wide voltage of 3.5 V and high areal capacitance of 17.4 mF cm<sup>-2</sup>, outperforming most carbon based MSCs [56]. Daeil et al. reported an air-stable and flexible MSCs by using poly(ethylene glycol) diacrylate/1-ethyl-3-methylimidazolium bis(trifluoromethyl sulfonyl)imide (PEGDA/[EMIM][TFSI]) electrolyte (Fig. 8a and b). Fig. 8c and d presented the MSCs under different bending states with good capacitance retention ability. Moreover, MSCs applying PEGDA/[EMIM][TFSI] as electrolyte were highly stable after 8 weeks in air (Fig. 8e) [100].

Although plenty of merits of lithium ion gel polymer electrolytes, proton conducting gel polymer electrolytes, alkaline gel polymer electrolytes, and ion gel polymer electrolytes have been discovered, there still exist key challenges limiting the energy/power density and cyclability for MSCs, including operating temperature window, ionic conductivity, thermal and chemical stabilities. In details, the operating voltage is narrow ( $<1.2$  V) and the operating temperature is in short ranges from 0 °C to 60 °C for lithium ion, proton and alkaline electrolytes due to the

existence of water [101]. The ionic gel polymer electrolytes endow a wider voltage window (up to 4 V). However, its ionic conductivity is one magnitude inferior to the proton gel polymer electrolytes. In addition, the ionic gel polymer electrolyte is sensitive to the trace amounts of water and metal ion contamination, which would lead to self-charge process and reduce the operating voltage window. Therefore, further study on advanced electrolyte should optimize the conductivity, operating voltage, and thermal stability to achieve a high-energy density and wide temperature applicable MSCs [102].

#### 2.4. Performance evaluation of flexible MSCs

The calculations of how much charge stored and how quickly the charge stored and released are crucial for practical applications of supercapacitors. The electrochemical performances parameters (capacitance, energy density and power density) of traditional supercapacitors are calculated according to the weight of electrodes. However, compared with the total weight of device, the electrodes weight of MSCs is negligible. Therefore, the volumetric energy density and power density are more suitable for evaluating the electrochemical performance of MSCs, providing comparable metrics for reported data regardless of their electrode thickness [8,14]. The specific capacitance (C), energy density (E), and power density (P) are obtained by the following equations. The capacitance could be calculated from the CV curves or GCD profiles in term of equation (1) or equation (2), respectively.

$$C = \frac{1}{\nu(V_f - V_i)} \int_{V_i}^{V_f} I(V) dV \quad (1)$$

$$C = \frac{I\Delta t}{(V_f - V_i)} \quad (2)$$

**Table 1**  
Recently reported electrode materials for flexible in-plane MSCs.

Electrode materials	Electrolyte	Cell voltage (V)	Areal capacitance (mF cm <sup>-2</sup> /mF cm <sup>-1</sup> )	Volume capacitance (mF cm <sup>-3</sup> )	Energy density (mWh cm <sup>3</sup> /mWh cm <sup>-2</sup> )	Power density (mW cm <sup>-3</sup> /mWh cm <sup>-2</sup> )	Refs
Graphene fibres	PVA/H <sub>2</sub> SO <sub>4</sub> gel	1	228 mF cm <sup>-2</sup>	114.5	4 mWh cm <sup>-3</sup>	–	[79]
SWNT@CHI fibres	PVA/H <sub>2</sub> SO <sub>4</sub> gel	0.8	37.1 mF cm <sup>-2</sup>	48.5	3.7 mWh cm <sup>-3</sup>	0.0457 mW cm <sup>-3</sup>	[89]
NG fibres	EMIBF <sub>4</sub> /PVDF-HFP gel	3	306.3 mF cm <sup>-2</sup>	–	46.9 mWh cm <sup>-2</sup>	1.5 mWh cm <sup>-2</sup>	[90]
CNT/Graphene fibres	PVA/H <sub>3</sub> PO <sub>4</sub> gel	1	116.3 mF cm <sup>-2</sup>	45	6.3 mWh cm <sup>-3</sup>	1085 mW cm <sup>-3</sup>	[77]
rGO/MWCNT fibres	PVA/H <sub>3</sub> PO <sub>4</sub> gel	1	42 mF cm <sup>-1</sup>	–	5.8 mWh cm <sup>-3</sup>	–	[78]
rGO	PVA/H <sub>2</sub> SO <sub>4</sub> gel	1	0.08 mF cm <sup>-2</sup>	17.9	2.5 mWh cm <sup>-3</sup>	495 W cm <sup>-3</sup>	[91]
m-MnO <sub>2</sub> /VN	SiO <sub>2</sub> -LiTFSI gel	2	16.1 mF cm <sup>-2</sup>	38.8	21.6 mWh cm <sup>-3</sup>	1.539 W cm <sup>-3</sup>	[32]
LIG-MnO <sub>2</sub>	PVA/LiCl gel	1	933.6 mF cm <sup>-2</sup>	92.4	3.2 mWh cm <sup>-3</sup>	0.23 W cm <sup>-3</sup>	[28]
LIG-PANI	PVA/H <sub>2</sub> SO <sub>4</sub> gel	0.8	360.8 mF cm <sup>-2</sup>	47.5	1.1 mWh cm <sup>-3</sup>	0.82 W cm <sup>-3</sup>	[28]
LIG-FeOOH//LIG-MnO <sub>2</sub>	PVA/LiCl gel	1.8	21.9 mF cm <sup>-2</sup>	5.4	2.4 mWh cm <sup>-3</sup>	2.89 W cm <sup>-3</sup>	[28]
GCP	PVA/H <sub>2</sub> SO <sub>4</sub> gel	0.8	107.5 mF cm <sup>-2</sup>	45.3	1.27 μW h cm <sup>-2</sup>	1.22 mW cm <sup>-2</sup>	[57]
EG-PANI	PVA/H <sub>2</sub> SO <sub>4</sub> gel	0.8	7.63 mF cm <sup>-2</sup>	36.8	3.14 mWh cm <sup>-3</sup>	1.14 W cm <sup>-3</sup>	[38]
EG//MP	PVA/LiCl gel	1.8	3.6 mF cm <sup>-2</sup>	14.6	6.58 mWh cm <sup>-3</sup>	1.46 W cm <sup>-3</sup>	[38]
PG	BMIMPF <sub>6</sub>	3	9.8 mF cm <sup>-2</sup>	37.5	11.6 mWh cm <sup>-3</sup>	1.5 W cm <sup>-3</sup>	[88]
PANI-G	PVA/H <sub>2</sub> SO <sub>4</sub> gel	1	210 mF cm <sup>-2</sup>	436	11.7 mWh cm <sup>-3</sup>	10.6 W cm <sup>-3</sup>	[92]
L-rGO	Na <sub>2</sub> SO <sub>4</sub>	1	0.51 mF cm <sup>-2</sup>	3.1	0.43 μW h cm <sup>-2</sup>	9.4 W cm <sup>-3</sup>	[20]
MXene	PVA/H <sub>2</sub> SO <sub>4</sub> gel	0.5	12 mF cm <sup>-2</sup>	562	0.31 μW h cm <sup>-2</sup>	11.4 μW cm <sup>-2</sup>	[50]
MXene	PVA/H <sub>2</sub> SO <sub>4</sub> gel	0.6	27.29 mF cm <sup>-2</sup>	119	6.1 mWh cm <sup>-3</sup>	–	[53]
g-C <sub>34</sub> N <sub>6</sub> -COF	LiCl/PVA gel	0.8	15.2 mF cm <sup>-2</sup>	–	7.3 mWh cm <sup>-3</sup>	0.05 W cm <sup>-3</sup>	[93]
AgNWs-MoS <sub>2</sub>	PVA/H <sub>2</sub> SO <sub>4</sub> gel	1.2	27.6 mF cm <sup>-2</sup>	–	2.453 μWh cm <sup>-2</sup>	1.472 mW cm <sup>-2</sup>	[94]
FG	EMIMBF <sub>4</sub> /PVDF-HFP gel	3.6	17.4 mF cm <sup>-2</sup>	134	56 mWh cm <sup>-3</sup>	21 W cm <sup>-3</sup>	[56]
Cu(OH) <sub>2</sub> @FeOOH	EMIBF <sub>4</sub> -SiO <sub>2</sub> gel	1.5	58 mF cm <sup>-2</sup>	32.2	18.07 μW h cm <sup>-2</sup>	–	[95]
LSG	EMIBF <sub>4</sub> -SiO <sub>2</sub> gel	2.5	–	2.35	19 mWh cm <sup>-3</sup>	141 W cm <sup>-3</sup>	[87]
RG0//RG0-MoO <sub>2</sub>	PVA/LiCl gel	1.4	7.9 mF cm <sup>-2</sup>	36.2	5.46 mWh cm <sup>-3</sup>	0.16 W cm <sup>-3</sup>	[24]
PNG//PNG-MoO <sub>2</sub>	PVA/LiCl gel	1.4	33.6 mF cm <sup>-2</sup>	152.9	38.1 mWh cm <sup>-3</sup>	0.8 W cm <sup>-3</sup>	[24]
MXenes	PVA/H <sub>2</sub> SO <sub>4</sub> gel	0.6	61 mF cm <sup>-2</sup>	–	0.63 μWh cm <sup>-2</sup>	0.33 mW cm <sup>-2</sup>	[49]
SPG	PVA/H <sub>3</sub> PO <sub>4</sub>	0.8	1 mF cm <sup>-2</sup>	–	1.81 mWh cm <sup>-3</sup>	297 W cm <sup>-3</sup>	[46]
Prussian-blue	PVA/H <sub>2</sub> SO <sub>4</sub> gel	1	4.69 mF cm <sup>-2</sup>	–	12.1 mWh cm <sup>-3</sup>	0.5 W cm <sup>-3</sup>	[96]

CNT: Carbon nanotubes; SWNT: Single-walled carbon nanotubes, CHI: chitosan; EMIBF<sub>4</sub>/PVDF-HFP: 1-ethyl-3-methylimidazolium tetrafluoroborate/poly (vinylidene fluoride-co-hexafluoropropylene), m-MnO<sub>2</sub>: mesoporous manganese dioxide, VN: vanadium nitride; LIG: laser-induced graphene, PANI: polyaniline; GCP: graphene/carbon nanotube/cross-linked PH1000 film; EG: electrochemically exfoliated graphene, MP: MnO<sub>2</sub> nanosheets; PG: Phosphorene and Graphene; PANI-G: polyaniline-graphene; COF: covalent organic frameworks; AgNWs: Ag nanowires; FG: Fluorine-Modified Graphene; LSG: laser scribe graphene; PNG: plasma reduced graphene; SPG: screen-printed graphene.

where  $v$  is the scan rate (V s<sup>-1</sup>), and  $V_f$  and  $V_i$  are the operating voltage window limits of CV curve.  $I$  refers to the voltammetry discharge current (A).  $\Delta t$  means discharge time (s).

Areal capacitance (mF cm<sup>-2</sup>) and volumetric capacitance (F cm<sup>-3</sup>) of the devices are calculated based on the area and volume of two electrodes according to formula (3) and (4):

$$C_{device}^{areal} = C/A_{device} \quad (3)$$

$$C_{device}^{volumetric} = C/V_{device} \quad (4)$$

The volumetric energy density  $E$  (Wh cm<sup>-3</sup>) and power density  $P$  (W cm<sup>-3</sup>) of the device are obtained from the equations:

$$E = \frac{1}{2} \times C_{device}^{volumetric} \times \frac{(V_f - V_i - IR)^2}{3600} \quad (5)$$

$$P = \frac{E}{\Delta t} \times 3600 \quad (6)$$

where  $IR$  is Ohmic drop.

### 3. Micro-supercapacitors powered integrated system for flexible electronics

#### 3.1. Micro-supercapacitors powered integrated system for photodetection

Photodetector is a kind of optoelectronic unit that function via converting absorbed photons into an electrical signal. High-performance

photodetector is greatly valued for the widely applications from fire detection, video imaging, biomedical imaging to night-vision and motion detection [103]. The commercially available photodetectors are mainly produced from bulky crystalline silicon or other 3D materials (Si/Ge heterojunctions, InGaAs semiconductor alloys) and assembled on rigid substrates [104,105]. However, the bulk volume, expensive and strict fabrication process hinder the bendable and stretchable applications. Currently, novel functional materials, such as 0D and 1D inorganic nanostructures, 2D layered materials and perovskite materials have been applied on flexible photodetectors, demonstrating excellent mechanical flexibility [106]. The processing methods were revolutionized to be more cost-effective. Combining the MSCs and photodetector in one single substrate as a flexible system is a potential strategy for future wearable and portable photodetecting applications.

Yang et al. demonstrated a scalable and effective method by using electrochemical deposition and ink printing to fabricate a flexible integrated system that contains a wireless charging coil, an asymmetric MSC and a photodetector in a single plane substrate as shown in Fig. 9a [36]. This system was autonomous via the wireless coil harvesting energy from a wireless power transmitter and charging the MSCs for powering the detector (Fig. 9b). High specific capacitance electrode materials, including V<sub>2</sub>O<sub>5</sub>-polyaniline (PANI) and MnO<sub>2</sub>-PPy, were used to achieve a high energy density of 20 mWh cm<sup>-3</sup> with a wide voltage output of 1.6 V. The integrated system also delivered good photoresponding properties. The photocurrent under light was much larger than that under the dark, suggesting the outstanding photoresponse of the perovskite nanowires (Fig. 9c). The MSCs based integrated system showed a comparable current on/off ratios of 1015 compared with external power-driven system

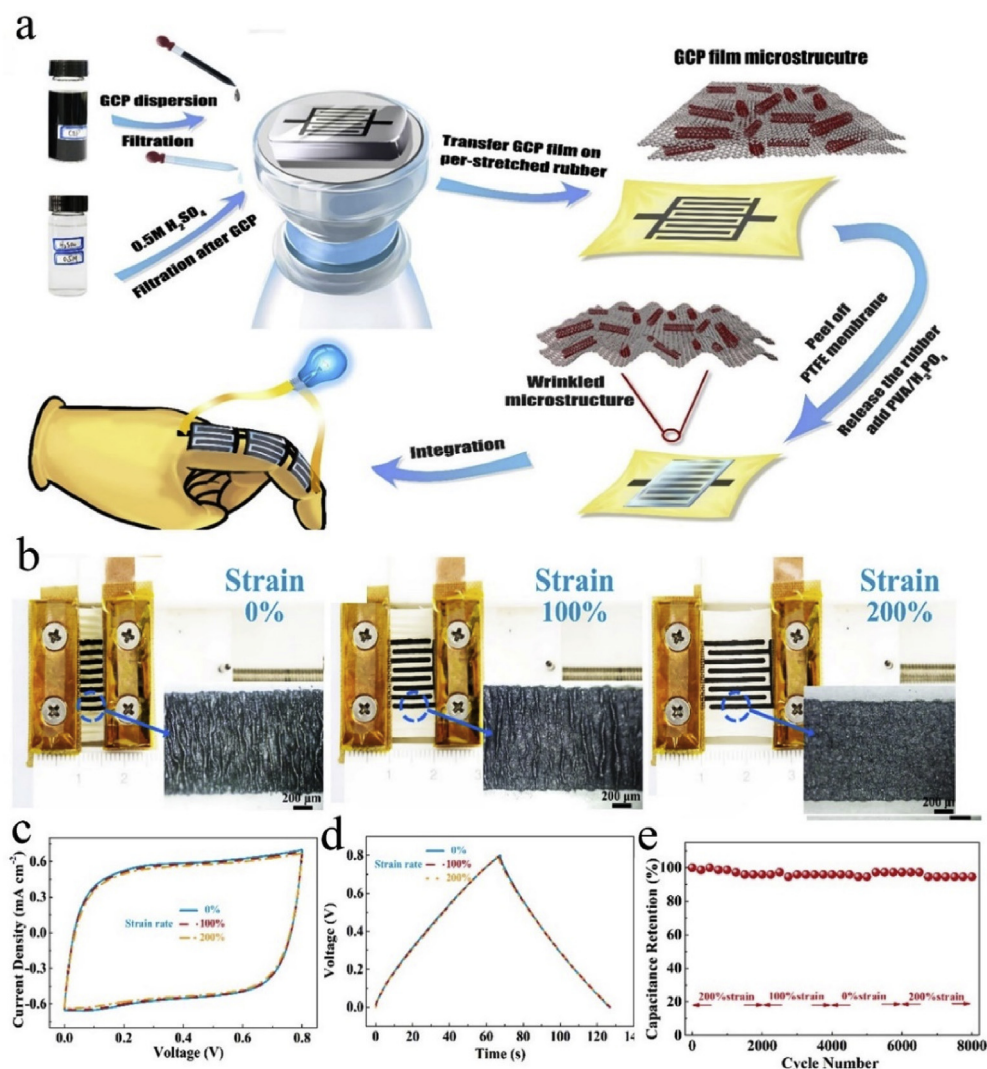


**Fig. 7.** (a) Schematic of the fabrication process of stretchable graphene/carbon nanotube/cross-linked PH1000 film MSCs (GCP-MSCs). (b) Stretchability test of GCP-MSCs. (c) CV, (d) GCD and (e) Cyclability of GCP-MSCs. Reproduced with permission from Ref. [57]. Copyright 2018 Elsevier.

current on/off ratios of 1054 [36]. Moreover, Yang et al. reported a 3D self-healable MSC integrated photodetector for light sensing, which advanced the practical applications in flexible electronics [107]. The self-healing property was favoured for extremely environment, corresponding to internal or external mechanical damage, which improved the reliability and stability of the device. Graphene and MXene nanocomposites were used as electrode materials and coated with a self-healing polyurethane (Fig. 9d and e). The obtained MSCs showed an outstanding capacitance of  $34.6 \text{ mF cm}^{-2}$  and good capacitance retention ability after fifth cycles healing tests. To demonstrate the practical application of self-healing MSCs, the MSCs were used to drive a photodetector of perovskite nanowires. The on/off ratio of the photodetector powered by original and healed MSCs was almost the same (Fig. 9f), indicating the reliability of the self-healing MSCs. Foldability is an important property for flexible electronics. Junyeong et al. developed a foldable MSCs integrated system for UV light detecting. Foldable substrate including polymers, fabric, paper, and cellulose nanofibers are also desired for future flexible electronics due to their cheaper cost, light weight, high safety, and robust mechanical stability under deformation [98]. Fig. 9g presented the novel design of foldable UV light sensor system. The system contains asymmetric micro-supercapacitors (AMSC) array and UV sensor integrated on a paper interconnected by liquid metal. The integrated system with good mechanical properties could bear

folded states without tearing or fracture. Excellent photocurrent was revealed after the repetitive folded and flat tests and the sensing function could last 1500 s (Fig. 9h). Shao et al. reported the fabrication of on-chip MSCs and photodetecting integrated devices on chip (Fig. 9i) [108]. To examine the photoresponse characteristics of CdS nanowire-based photodetector driven by MSCs, a 470 nm light with various power intensities was applied to illuminate the detector. Fig. 9j presented that the saturated photocurrent increases depend on increasing light density, suggesting the excellent reproducibility of the completely integrated system.

### 3.2. Micro-supercapacitors powered integrated system for gas sensing

Portable and wearable electronics with function of molecular monitoring have attracted tremendous attention for personal medical health [109]. Gas sensors are extremely important for detecting gas molecules, including ammonia, nitric oxide, which are toxic and have potential risk to human health [110]. However, commercial gas sensors are fail to meet the properties of low cost, light weight, good flexibility and stretchability, which are highly crucial for portable and wearable electronics [111]. Recently, integrating soft gas sensors with micro-supercapacitors on a flexible substrate is an effective and reliable strategy to realize the wearable and real time gas monitoring function.

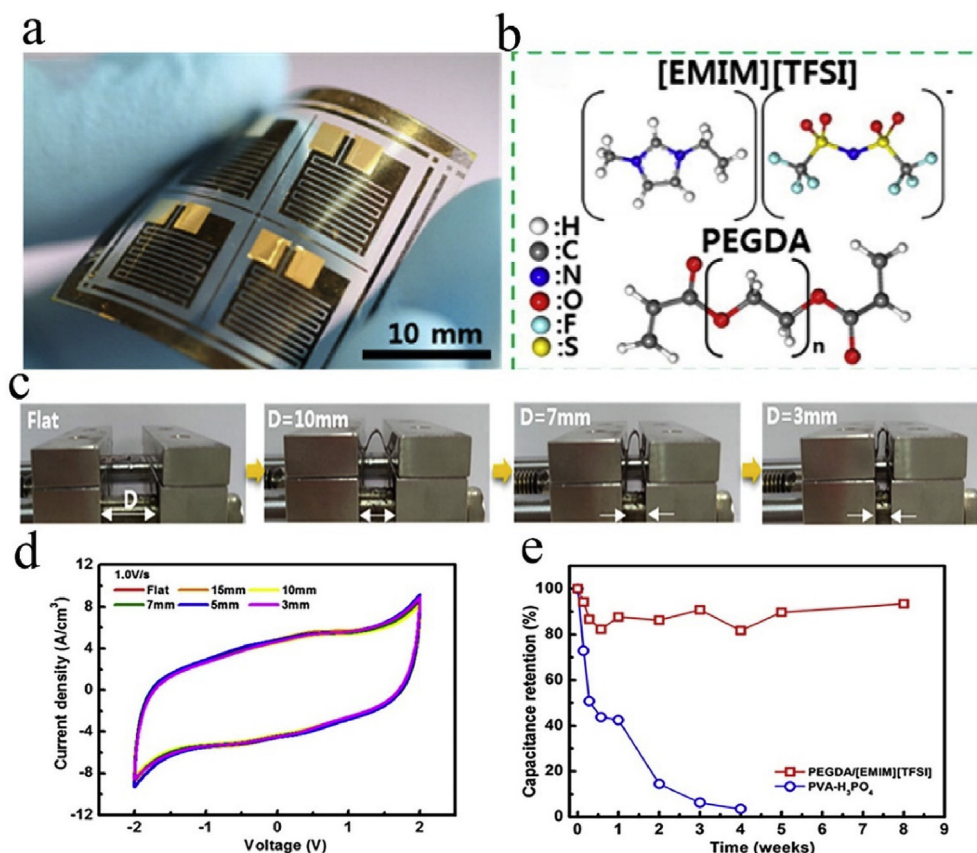


**Fig. 8.** (a) Photo of MSCs patterned on PET substrate. (b) Molecular structure of [EMIM][TFSI] and PEGDA. (c) Photos of bending tests of MSCs. (d) CV curves under different bending tests. (e) Capacitance retentions of MSCs with PVA/ $H_3PO_4$  and PEGDA/[EMIM][TFSI]. Reproduced with permission from Ref. [100]. Copyright 2015 American Chemical Society.

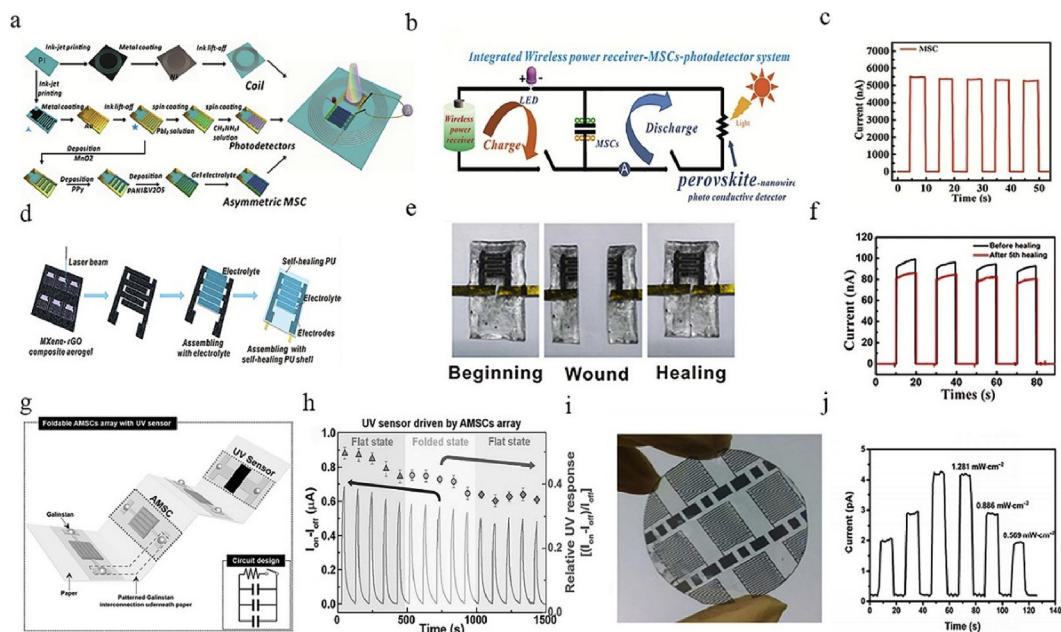


**Fig. 9.** (a) Illustration of the fabricating process of flexible asymmetric MSCs integrated with photodetector. (b) Circuit diagram of the integrated system. (c) Photoresponse of the integrated system under illumination on/off states. Reproduced with permission from Ref. [36]. Copyright 2016 American Chemical Society. (d) Schematic diagram of fabricating process of self-healing MSCs. (e) Photographs of the self-healing MSCs under cutting test. (f) Photoresponse behavior driving by original and self-healing MSCs. Reproduced with permission from Ref. [107]. Copyright 2018 American Chemical Society. (g) Schematic illustration of foldable MSCs integrated with UV sensor on a piece of paper. (h) Photoresponse of the photodetectors under folded and flat states. Reproduced with permission from Ref. [98]. Copyright 2017 WILEY-VCH. (i) Photograph of scalable MSCs integrated system on a wafer (j) Photoresponse of photodetector under various illuminating power. Reproduced with permission from Ref. [108]. Copyright 2015 WILEY-VCH. Tsinghua University Press and Springer-Verlag Berlin Heidelberg.

Junyeong et al. developed a deformable gas sensor-MSC integrated system (Fig. 10a) [112]. Materials for fabricating the integrated system, including the multi-walled CNT and polyaniline as electrode materials, PEDGA/[EMIM][TFSI] as ion-gel electrolyte, gold wire as interconnection conductor, graphene as gas sensor material, ecoflex and SU8 as soft substrate, enabled full degree deformation of the device. The whole device under 40% biaxial strain could keep the device integrity without any cracks (Fig. 10b), indicating the excellent mechanical properties. The CV curves almost overlapped under various biaxial strains (Fig. 10c), suggesting negligible effect on MSCs electrochemical performance by the deformation. In addition, the sensing mechanism of graphene gas sensor is illustrated in Fig. 10d.  $\text{NO}_2$  molecule was a strong oxidizer which will withdraw electrons from graphene, contributing enhanced electrical conductivity when graphene absorbs the  $\text{NO}_2$  [112]. Figs. 10e and f showed the sensing performance under applied uniaxial strain of up to 50% powered by external power supply of 1 V and MSCs array, respectively. A gradually decrease with time up to 50 min and sensitivity almost without changing were observed for both systems, clearly indicating that the integrated MSCs are capable to power the patterned-graphene sensor under stretch condition. La et al. reported a wearable gas sensor-MSC array and PCB system [113]. The system could be worn on the athlete wrist (Fig. 10g and h). The real time detecting function was presented with different concentration value of  $\text{C}_2\text{H}_5\text{OH}$  on a mobile phone (Fig. 10h). Fig. 10i revealed the sensing mechanism of MWCNTs/PANI

sensor. The  $\text{C}_2\text{H}_5\text{OH}$  molecule was exposed to the gas sensor and reacted with  $\text{O}_2$  to form  $\text{CO}_2$  and  $\text{H}_2\text{O}$ . The released electrons decreased hole concentration of MWCNTs and in-situ reduced PANI into emeraldine salt, resulting the increase of conductivity of the active layers [113]. The superior gas detecting performances were verified via the uniform current response of gas sensor at concentration of 50 ppm (Fig. 10j) and the continuous increase of current density as the concentrations ranging from 1 to 200 ppm (Fig. 10k). Furthermore, the gas sensor kept the same current response under repeat bendings (Fig. 10l). Besides, the integrated system could detect various kinds of gas, such as methanol, dimethyl formamide, and acetone, etc (Fig. 10m). Rui et al. reported paper as a substrate for integrating MSC, gas sensor and solar cell [114]. Compared with polymer substrate, paper was a promising flexible substrate due to its cheap, abundant and disposable properties. The integrated system can bear 10,000 bending cycles without electrochemical and sensing degradations. This sustainable and self-powered integrated device based on MSCs could be transferred to various type textiles, indicating the great potential on wearable electronics.

### 3.3. Micro-supercapacitors powered integrated system for motion monitoring

Wearable strain sensors for monitoring subtle human motion is an important part of flexible electronics due to the wide applications on

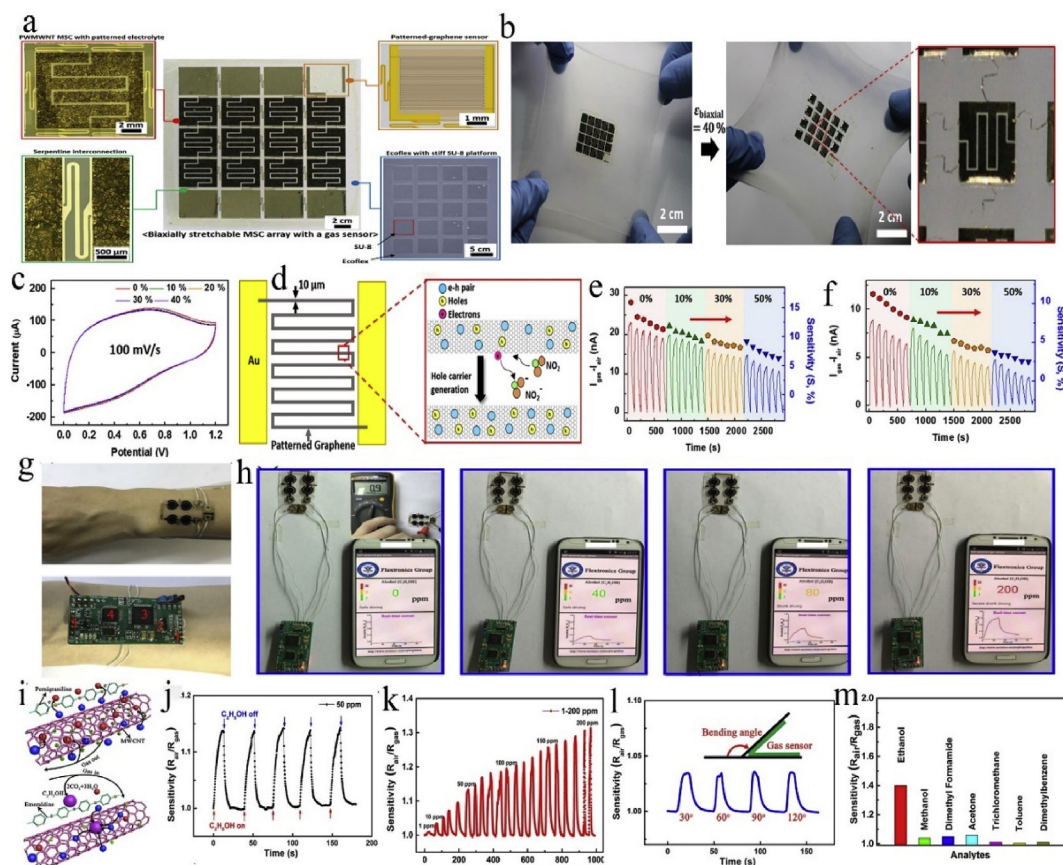


**Fig. 10.** (a) Photograph of biaxially stretchable patterned-graphene sensor integrated with a polyaniline-wrapped multi-walled carbon nanotube (PVMWNT) MSC array. (b) Photograph of the integrated system under 40% biaxial stretching. (c) CV curves of MSCs under strain tests. (d) Illustration of graphene base gas sensor and mechanism for detecting  $\text{NO}_2$  gas. (e and f) Current response of graphene based gas sensor under repeat exposure of 200 ppm  $\text{NO}_2$  by applying an external power supply and an integrated MSCs, respectively. Reproduced with permission from Ref. [112]. Copyright 2015 Elsevier. (g) Photographs of flexible MSCs integrating with gas sensor and printed circuit board (PCB) on wrist. (h) Real time analysis of unknown concentration gas including no gas, low, middle and high concentrations of  $\text{C}_2\text{H}_5\text{OH}$ . (i) Mechanism of MWCNT/PANI nanocomposites gas sensor for detecting  $\text{C}_2\text{H}_5\text{OH}$  gas. (j) Stability test of MWCNT/PANI sensor under 50 ppm  $\text{C}_2\text{H}_5\text{OH}$  gas at room temperature. (k) Current response of MWCNT/PANI sensor to  $\text{C}_2\text{H}_5\text{OH}$  gas at different concentrations. (l) Repeated response of MWCNT/PANI sensor under bending test. (m) Sensor selectivity by exposing the device to different targeted gases at the same concentration. Reproduced with permission from Refs. [113]. Copyright 2017 Elsevier.

entertainment, medical, and sports industries [115–117]. For practical applications, the wearable sensor should be lightweight, thin, and sensitive, but needs extra power source. Integrating MSCs and strain sensors on one flexible substrate is very useful for the fabrication of maintain-free motion monitoring sensor.

As a presentative example, Junyeong et al. reported a stretchable solar cell-MSCs-strain sensor integrated system for skin-attachable health-monitoring devices (Fig. 11a) [118]. The working mechanism of strain sensor relied on the changes of contact resistance with applied stretching force. The elongated length of the sensor led to an increase of contact resistance over a large Area (Fig. 11b). Fig. 11c presented the resistance linearly increased from 134 to 193 KΩ with the applied strains varying from 0 to 30%. The integrated system could real-time detect the motion of wrist pulse and bending (Fig. 11d and e). The uniform pulse signal was monitored for the system with 15 beats per 10 s for a uniform interval pulse, regardless of the charging method, such as by external power, solar simulator, and solar light (Fig. 11f). Similar to wrist motion, the resistance response of bending motion was similar and the resistance increased from 134 to 145 kΩ and back to 134 kΩ (Fig. 11g), suggesting the reliability of the system. Furthermore, the integrated system demonstrated excellent stability after 1000 repetitive biaxial stretching/releasing cycles with no noticeable change. In addition, Yu et al. designed a vertical stacked MSCs-piezoresistance sensor for static pressure sensing and dynamic tactile trajectory [119]. Fig. 11h illustrated the all-in-one system consisted of two parts. MSCs worked as energy storage units and piezoresistance sensor played as function part. Porous CNT-PDMS was used for both electrode materials of MSCs and sensing materials for piezoresistance sensor. The piezoresistive-sensing patch demonstrated excellent performances that resistance value lineally increased with the expanded bending angles (Fig. 11i) and periodic

resistance responses were accordance with repeated muscle motions (Fig. 11j) In addition, the device could apply on personal identification and safety communication applications (Fig. 11k and l). Fig. 11k exhibited the touching habit of each person by presenting user’s touching force on the sensor. The user pressed the piezoresistance sensor to login the program by judging the number and interval time. These demonstrated that the 3D touch is a promising tool for user identification and safety communication in future.

### 3.4. Micro-supercapacitors powered integrated system for body fluid monitoring

Sweat is one of important human’s biomarkers due to its rich metabolically and physiologically information. Sweat analysis is now broadly applied for various applications, including drug abuse detection, disease diagnosis, and athletic performance optimization [2,120]. However, these applications contained individual sweat collection/storage and sample analysis process. Commercial facility failed to meet the real time analysis of sweat content secretion. Recently, portable and wearable sweat sensors integrated with multi-functioned biosensors have triggered enormously interest. MSC is an effective and low-cost energy storage unit, which can be integrated with the sweat biosensors on a soft substrate to fulfil the goal of real time and maintains free analysis.

For instance, Yao et al. reported a self-powered enzyme-free sweat monitoring system with integrated MSCs [121]. The monitoring system was arranged on a PET substrate by conventional photolithography and electron-beam evaporation process with three parts, including NiCo<sub>2</sub>O<sub>4</sub>/chitosan based glucose sensor, ion selective membrane based [Na<sup>+</sup>] and [K<sup>+</sup>] selective sensors, and NiCo<sub>2</sub>O<sub>4</sub>-based MSCs which could be easily attached on human wrist or ankle (Fig. 12a–c). The device

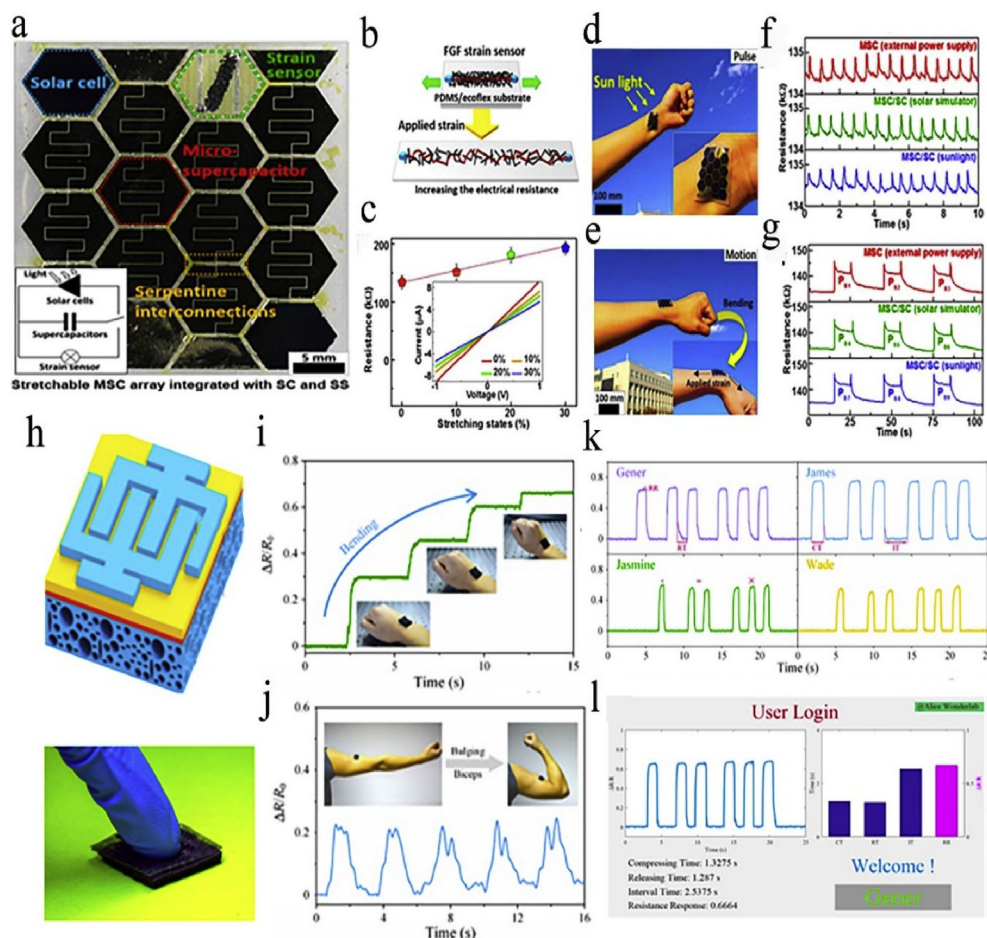
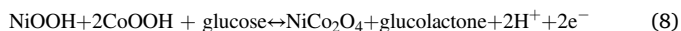


Fig. 11. (a) Photograph of the stretchable MSC array, solar cell and strain sensor integrated on a soft ecoflex substrate. (b) Strain sensing mechanism. (c) Resistance response to applied strain. Inset is I-V curves of strain sensor under various stretching states. (d, e) Photograph of integrated device on human wrist for testing pulse and bending motion, respectively. (f, g) Resistance response of strain sensor under pulse and bending motion states powered by external power, solar simulator, and MSC, respectively. Reproduced with permission from Refs. [118]. Copyright 2018 Elsevier. (h) Schematic illustration and photograph of all-in-one device, including piezoresistance sensor and MSCs. (i and j) Photograph and resistance response of the device for monitoring arm and muscle movements, respectively. (k) Four persons footprint of recorded resistance responses of 3D touch with the same compressing process, one touch for “.”, two touches for “-”, and three touches for “×”. (l) Login program through personal recorded resistance response for user identification. Reproduced with permission from Refs. [119]. Copyright 2018 Elsevier.

delivered a high areal capacitance of  $18.5 \text{ mF cm}^{-2}$  and excellent sensitivities of  $0.5 \mu\text{A}/\mu\text{M}$  for glucose,  $0.031 \text{ nF}/\text{mM}$  for  $[\text{Na}^+]$  and  $0.056 \text{ nF}/\text{mM}$  for  $[\text{K}^+]$ . Figs. 12d and e presented the glucose sensor current response with various concentrations ranging from 10 to  $200 \mu\text{M}$  and  $[\text{K}^+]$  sensor at varied concentrations of 1–16 mM, respectively, indicating the wide ranges of detection sensitivities. The mechanism for glucose detection was according to the following equations.



The glucose could react with NiOOH to form glucolactone during the detecting process. The produced redox current was dependent on the glucose concentration. As the increase of sweat volume, the glucose concentration was also increased and more glucose molecules reacted with NiOOH, resulting in the increase of the response current. When the sensor analysed the current induced by inorganic ions ( $\text{Na}^+$  and  $\text{K}^+$  et al.) in sweat, the ions would influence the sensitivity interactively due to the similarity of two ions charge and molecular weight. A compensation electrode was applied through insulating the electrodes by using a membranes, suggesting the reliability of the obtained data [121]. Similarly, a linear relationship of  $[\text{Na}^+]$  and  $[\text{K}^+]$  concentrations and response current were observed. The system could real-time monitoring of an athlete sweat contents of glucose and  $\text{K}^+$  ions (Fig. 12f and g). The response of the sensor system in monitoring glucose and  $\text{K}^+$  ions in sweat gradually increased from 31.5 to  $116.3 \mu\text{A}$  and  $0.02$ – $1.08 \text{ nF}$  with the prolonging of exercise time, respectively. Furthermore, the wearable

sensor device was integrated with WIFI module, microcontroller and android phone for the real time analysis displaying the athlete sweat content (Fig. 12h). The current densities values of glucose,  $[\text{Na}^+]$  and  $[\text{K}^+]$  were increased with the continuous exercise of athlete. The red fonts of the words in Fig. 12h indicated the volunteer in subhealth state needing supplement water.

### 3.5. Micro-supercapacitors powered integrated system for micro-LED

LED is an important light source and has crucial applications on various fields. Especially, the micro-LED is highly suitable for flexible electronics, such as wearable watches, automotive head, augmented reality (AR)/visual reality (VR), mobile phones-up displays, high-end televisions, and micro projectors. Integrating with MSCs as a micro-power source can realize the self-power purpose and reduce the weight of the total device [122].

Hyoungjun et al. developed a stretchable array MSCs- $\mu$ -LEDs device with waterproof function. Fig. 13a showed the fabrication process by photolithography and e-beam technology [123]. The functionalized MWNTs were used as electrode materials, and the whole device was encapsulated in thin Ecoflex polymer. The integrated device has not only the stretchability but also waterproof function, which are important for flexible electronics applications in harsh environments, such as raining or snowing. The device under flat, bend, winding, stretching, and twisting states in water could still illuminate  $\mu$ -LEDs without noticeable brightness degradation (Fig. 13b). The CV curves in Fig. 13c were almost overlapped, confirming the stability of MSCs. Yein et al. also reported a

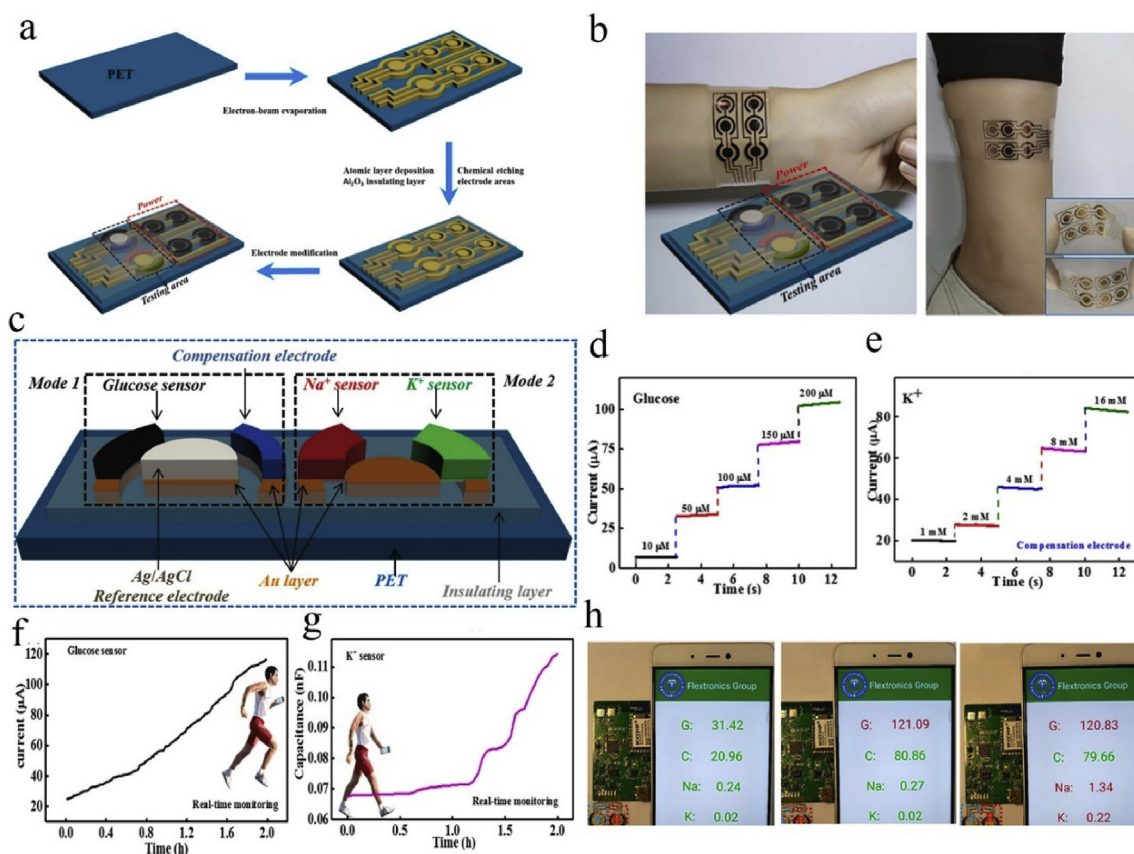


**Fig. 12.** (a) Illustration of fabricating process of self-powered sweat monitoring system. (b) Photographs of the integrated device on the human wrist and ankle. (c) Details for sensor arrays, including glucose sensor and compensation electrode sensors. Mode 1 and Mode 2 are amperometric sensor and capacitance-type sensor, respectively. (d and e) Current responses of glucose sensor and  $\text{K}^+$  sensors, respectively. (f and g) Current responses of real-time monitoring of athlete sweat Contents of glucose and  $\text{K}^+$  ions, respectively. (h) The real time analysis and display the sweat contents of glucose (G) compensation electrode (C),  $\text{Na}^+$  (Na), and  $\text{K}^+$  (K) in the case of before movement and after movement. Reproduced with permission from Ref. [121]. Copyright 2019 Elsevier.

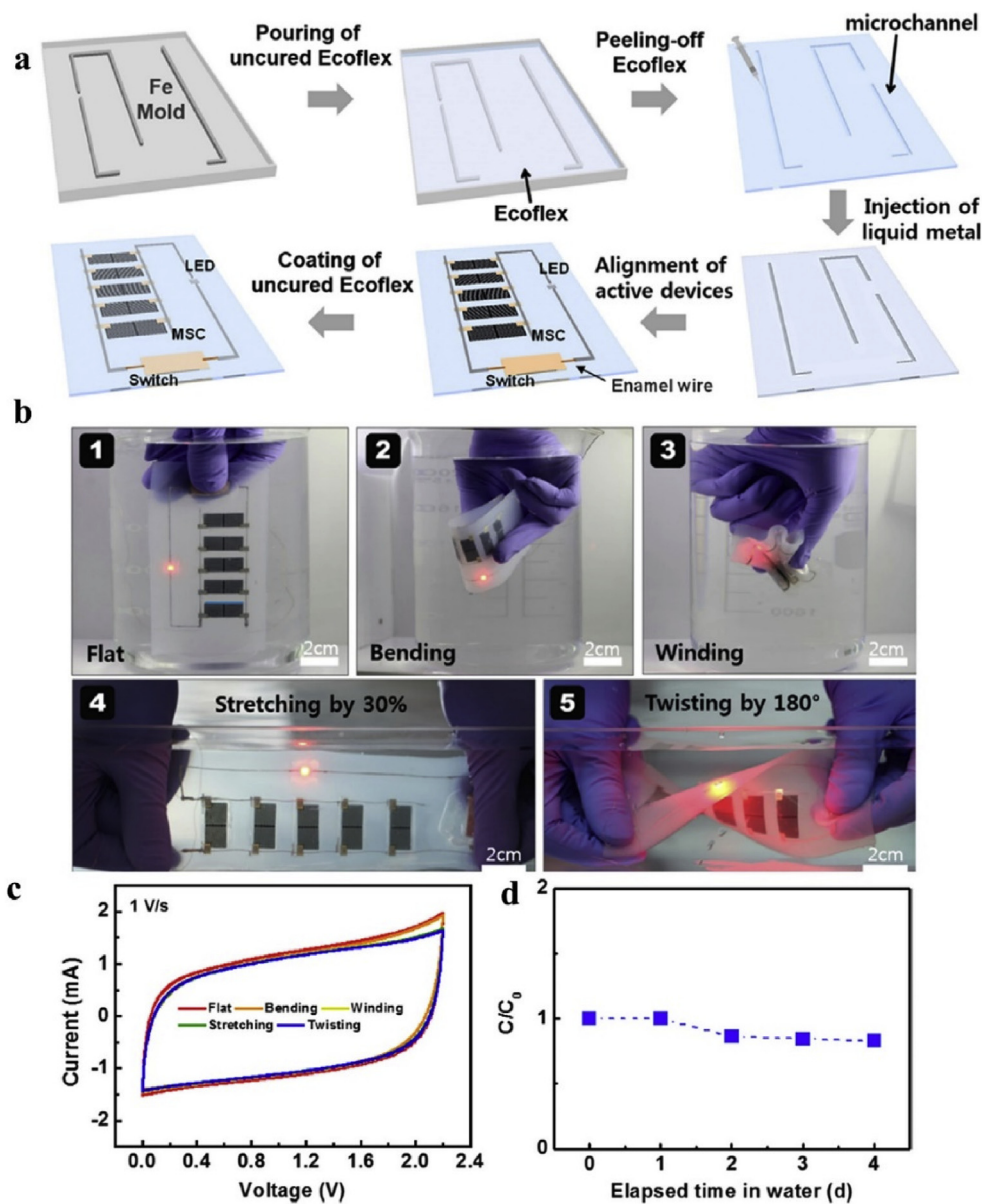


**Fig. 13.** (a) Schematic illustration of fabrication of the stretchable water-proof MSCs array with micro-LED ( $\mu$ -LED). (b) Photographs of the integrated device under various deformations in water. (c) CV curves recorded under various deformation states. (d) Normalized capacitance ( $C/C_0$ ) measured in water for 4 d. Here,  $C_0$  and  $C$  are the capacitances before and after immersion in water, respectively. Reproduced with permission from Ref. [123]. Copyright 2016 American Chemical Society.

deformable MSCs- $\mu$ -LEDs device [124]. The fabrication process was layer-by-layer method and the obtained MSCs delivered a high energy density of  $25 \text{ mWh cm}^{-3}$ . The MSCs arrays could light  $2 \times 2 \mu$ -LEDs under 50% biaxial stretching. Furthermore, Kim et al. fabricated a flexible MSCs array- $\mu$ -LEDs device by using all solid state materials, including SWCNT electrodes, ionic liquid-based triblock copolymer electrolyte, and long serpentine metallic interconnections [125]. The integrated MSCs array- $\mu$ -LEDs system was washingly stable even under bending or stretching without deteriorations. Wen et al. reported flexible asymmetric MSCs integrated with bookmark light with good mechanical stability [126]. The asymmetric MSCs were produced by using screen printed the  $\text{MoO}_{3-x}$  nanorods as positive fingers, activated carbon nanospheres for negative fingers and sodium alginate bio-hydrogel as electrolytes (Fig. 14a). The asymmetric MSCs presented high areal capacitance of  $47.20 \text{ mF cm}^{-2}$  and superior energy density of  $21.20 \mu\text{Wh cm}^{-2}$ . The MSCs have shown good flexibility even under  $180^\circ$  bending test without any damages of the device (Fig. 14b). The MSCs integrated on printed circuits could sufficiently power the bookmark light under

bending states (Fig. 14c), indicating promising applications for customized power systems in the portable and wearable on-chip electronics.

#### 4. Perspective and research challenges

Flexible electronics have aroused huge attentions on providing enhanced smart functions and giving health information by monitoring body and environments conditions. This review summarized latest advances of in-plane MSCs and MSCs as microscale energy storage units of integrated systems for wearable and portable electronics. The electrode materials, electrolyte, performance evaluation metrics were precisely discussed. Various fabrication methods for flexible MSCs were also included to highlight their merits, including scalability, low production cost, and high effectiveness. Notably, MSCs as promising energy storage units were utilized for powering various sensors and electrical devices in flexible units. MSCs based integrated systems were introduced for the applications in flexible electronics, such as gas sensing, photodetecting, motion monitoring, body fluid monitoring, and micro-LED powering.

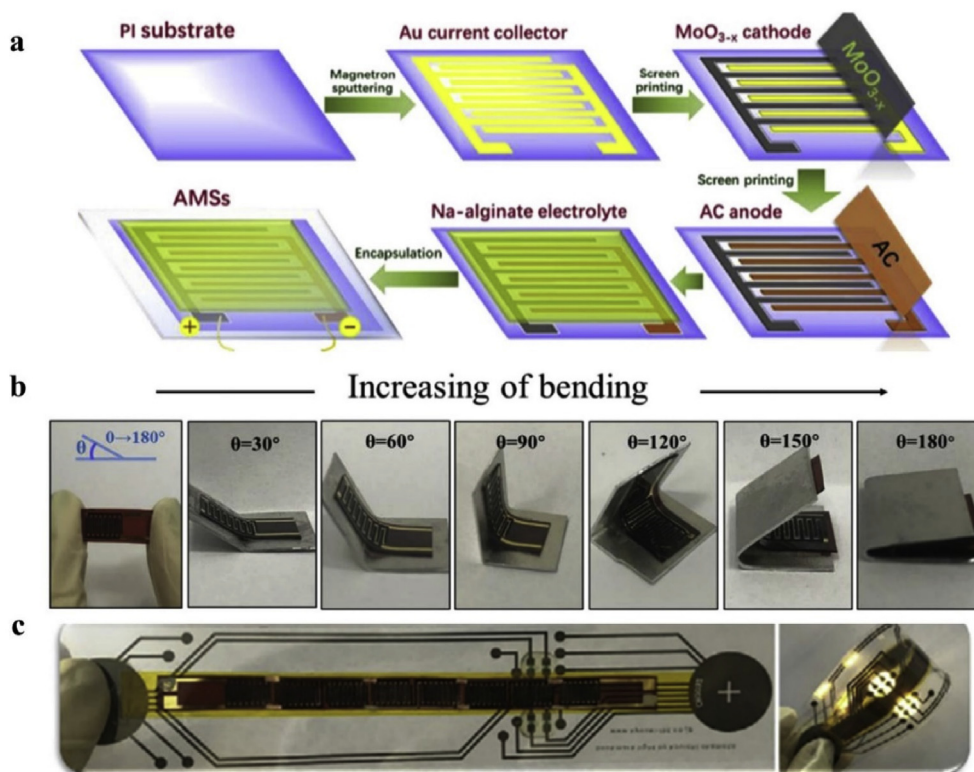


**Fig. 14.** (a) Schematic of fabricating MSCs. (b) Photographs of flexibility tests of MSCs under different bending angles from  $0^\circ$  to  $180^\circ$ . (c) Photographs of integrated MSCs integrated with  $\mu$ -LED device. Reproduced with permission from Ref. [126]. Copyright 2019 Elsevier.

However, there are still lots of opportunities along with challenges by developing fully integrating, wirelessly operating and self-powering micro systems.

To fulfil the purpose of MSCs as high energy and flexible energy storage units, some key challenges are still need to be solved as follows. First, new type high-performance electrode materials are demanded to improve the capacitance behaviour of the MSCs. To meet the requirement of flexible properties, thin-film based 2D electrode materials, such as graphene and MXenes, were intensively studied. There are still plenty of 2D materials as electrode materials for MSCs, such as 2D transition metal dichalcogenides, graphyne, 2D MOF, and 2D COF. However, most of these materials suffer poor conductivity and self-restacking between interlayers, which hinder charge transfer and limit their energy storage performance. Therefore, improving the electrical conductivity of these 2D layered materials and preventing the restacking of 2D nanosheets are crucial to achieve high energy density of MSCs. Nanocomposites of combing 2D layers with conductive 1D nanowires or 0D nanodots are promising for electrode materials. Specifically, MXenes reinforcing with polymer nanocomposites are of great promise for MSCs applications due to their high electrical conductivity, large capacitance, compressive strength, and excellent flexibility. Second, to meet the high voltage output of the flexible electronics for practical application, electrolytes with wide voltage operation window are still few. Most flexible electrolytes are based on proton conducting gel polymer electrolytes that suffer the water evaporation during the cycling test and narrow voltage window ( $<1$  V), leading to the unstable electrochemical performances and limited low energy density. Ion-gel electrolytes synthesised by mixing ion liquid with solid component (e.g. silica, polymer) have triggered enormous attention due to ultra-wide voltage window for sandwich type supercapacitors (typically, 3–4.5 V). However, ion-gel electrolytes are rarely studied for high-voltage MSCs. Therefore, developing new kinds of ion-gel electrolytes with high ions conductivity and flexibility to get wide voltage window and energy density for MSCs is a promising strategy to achieve high energy density. Third, scalable and

cheap fabrication technology for miniaturized MSCs with high resolution is still challenging. The package of current collectors, electrodes, electrolyte, substrate, and electronic component is the core part for the integrity and stability of high-performance of MSCs powered integrated flexible electronics under repeated deformation states. It requires that the fabrication method to optimize the interfacial interactions of electrolyte and electrodes, fabricate high-stacked 2D nanostructures to improve the ion diffusion and charge transfer, and enable the good connection of MSCs with other components to deliver the current signal. To fulfil this goal, printing technologies which enable high-throughput and large-area production of MSCs and sensors are showing great promise. Finally, the reported MSCs based integrated systems are still few which are unable to meet the huge demands of real-time, continuous and fast detection of individual's dynamic health status. Therefore, advanced types of MSCs based integrated systems should be developed to analyse in saliva, tears, sweat, blood, interstitial fluid, and exhaled breath. MSCs integrated systems transferred the data to mobile phone, smart watch, and other wearable displays to demonstrate information directly need to be more convenient, smart and quick. Importantly, the MSCs integrated systems for flexible electronics request the interdisciplinary research collaborations, which is benefiting greatly from the cross-fertilization between different research areas, such as materials science, biomedical engineering, electrical engineering, and energy research communities.

#### CRediT authorship contribution statement

**Liangzhu Zhang:** Writing - original draft. **Dan Liu:** Supervision, Writing - review & editing. **Zhong-Shuai Wu:** Supervision, Writing - review & editing. **Weiwei Lei:** Supervision, Writing - review & editing.

#### Declaration of competing interest

The authors declare no competing financial interest.

## Acknowledgements

This work was financially supported by the Australian Research Council Discovery Program (DP190103290) and Australian Research Council Discovery Early Career Researcher Award scheme (DE150101617). National Key R@D Program of China (Grants 2016YBF0100100), DICP I202032, National Natural Science Foundation of China (Grants 51572259, 51872283, and 21805273), Liao Ning Revitalization Talents Program (Grant XLYC1807153), Natural Science Foundation of Liaoning Province, Joint Research Fund Liaoning-Shenyang National Laboratory for Materials Science (Grant 20180510038), DICP (DICP ZZBS201708, DICP ZZBS201802), DICP&QIBEBT (Grant DICP&QIBEBT UN201702), Dalian National Laboratory For Clean Energy (DNL), CAS, DNL Cooperation Fund, CAS (DNL180310, DNL180308, DNL201912, and DNL201915). Liangzhu Zhang thanks for reviewer's efforts and suggestions on improving the quality of this review.

## References

- [1] J. Xu, H.-C. Wu, C. Zhu, A. Ehrlich, L. Shaw, M. Nikolka, S. Wang, F. Molina-Lopez, X. Gu, S. Luo, D. Zhou, Y.-H. Kim, G.-J.N. Wang, K. Gu, V.R. Feig, S. Chen, Y. Kim, T. Katsumata, Y.-Q. Zheng, H. Yan, J.W. Chung, J. Lopez, B. Murrmann, Z. Bao, *Nat. Mater.* 18 (2019) 594–601.
- [2] W. Gao, S. Emaminejad, H.Y.Y. Nyein, S. Challa, K. Chen, A. Peck, H.M. Fahad, H. Ota, H. Shiraki, D. Kiriya, D.-H. Lien, G.A. Brooks, R.W. Davis, A. Javey, *Nature* 529 (2016) 509–514.
- [3] D. Son, J. Kang, O. Vardoulis, Y. Kim, N. Matsuhisa, J.Y. Oh, J.W.F. To, J. Mun, T. Katsumata, Y. Liu, A.F. McGuire, M. Krason, F. Molina-Lopez, J. Ham, U. Kraft, Y. Lee, Y. Yun, J.B.H. Tok, Z. Bao, *Nat. Nanotechnol.* 13 (2018) 1057–1065.
- [4] L. Li, Z. Wu, S. Yuan, X.-B. Zhang, *Energy Environ. Sci.* 7 (2014) 2101–2122.
- [5] J. Song, X. Feng, Y. Huang, *Nat. Sci. Rev.* 3 (2015) 128–143.
- [6] Y. Lee, J.Y. Oh, W. Xu, O. Kim, T.R. Kim, J. Kang, Y. Kim, D. Son, J.B.H. Tok, M.J. Park, Z. Bao, T.-W. Lee, *Sci. Adv.* 4 (2018) 7387.
- [7] S. Wang, J. Xu, W. Wang, G.-J.N. Wang, R. Rastak, F. Molina-Lopez, J.W. Chung, S. Niu, V.R. Feig, J. Lopez, T. Lei, S.-K. Kwon, Y. Kim, A.M. Foudeh, A. Ehrlich, A. Gasperini, Y. Yun, B. Murrmann, J.B.H. Tok, Z. Bao, *Nature* 555 (2018) 83–88.
- [8] N.A. Kyremateng, T. Brousse, D. Pech, *Nat. Nanotechnol.* 12 (2017) 7–15.
- [9] Y. Wang, L. Sun, C. Wang, F. Yang, X. Ren, X. Zhang, H. Dong, W. Hu, *Chem. Soc. Rev.* 48 (2019) 1492–1530.
- [10] T. Lv, M. Liu, D. Zhu, L. Gan, T. Chen, *Adv. Mater.* 30 (2018) 1705489.
- [11] F. Yi, H. Ren, J. Shan, X. Sun, D. Wei, Z. Liu, *Chem. Soc. Rev.* 47 (2018) 3152–3188.
- [12] S. Zheng, X. Shi, P. Das, Z.S. Wu, X. Bao, *Adv. Mater.* (2019) 1900583.
- [13] B.D. Boruah, *Energy Storage Mater.* 21 (2019) 219–239.
- [14] C. Lethien, J. Le Bideau, T. Brousse, *Energy Environ. Sci.* 12 (2019) 96–115.
- [15] J. Hao, J. Wang, S. Qin, D. Liu, Y. Li, W. Lei, *J. Mater. Chem.* 6 (2018) 8053–8058.
- [16] Z.Y. Wang, S. Qin, S. Seyedini, J. Zhang, J.M. Wang, A. Levitt, N. Li, C. Haines, R. Ovalle-Robles, W.W. Lei, Y. Gogotsi, R.H. Baughman, J.M. Razal, *Small* 14 (2018) 1802225.
- [17] P. Simon, Y. Gogotsi, B. Dunn, *Science* 343 (2014) 1210–1211.
- [18] Y. Gogotsi, P. Simon, *Science* 334 (2011) 917–918.
- [19] P. Huang, C. Lethien, S. Pinaud, K. Brousse, R. Laloo, V. Turq, M. Respaud, A. Demortière, B. Daffos, P.L. Taberna, B. Chaudret, Y. Gogotsi, P. Simon, *Science* 351 (2016) 691–695.
- [20] W. Gao, N. Singh, L. Song, Z. Liu, A.L.M. Reddy, L. Ci, R. Vajtai, Q. Zhang, B. Wei, P.M. Ajayan, *Nat. Nanotechnol.* 6 (2011) 496–500.
- [21] J. Wang, F. Li, F. Zhu, O.G. Schmidt, *Small Methods* 3 (2019) 1800367.
- [22] W. Lei, S. Qin, D. Liu, D. Portehault, Z. Liu, Y. Chen, *Chem. Commun.* 49 (2013) 352–354.
- [23] L. Zhang, G. Yang, Z. Chen, D. Liu, J. Wang, Y. Qian, C. Chen, Y. Liu, L. Wang, J. Razal, *J. Mater. Chem.* 6 (2020) 138–144.
- [24] L. Zhang, Z. Chen, S. Zheng, S. Qin, J. Wang, C. Chen, D. Liu, L. Wang, G. Yang, Y. Su, Z.S. Wu, X. Bao, J. Razal, W. Lei, *J. Mater. Chem.* 7 (2019) 14328–14336.
- [25] D.W. Wang, F. Li, Z.-G. Chen, G.Q. Lu, H.-M. Cheng, *Chem. Mater.* 20 (2008) 7195–7200.
- [26] Z.S. Wu, Y. Zheng, S. Wang, C. Sun, K. Parvez, T. Ikeda, X. Bao, K. Müllen, X. Feng, *Adv. Mater.* 29 (2017) 1602960.
- [27] H. Li, Y. Hou, F. Wang, M.R. Lohe, X. Zhuang, L. Niu, X. Feng, *Adv. Energy Mater.* 7 (2017) 1601847.
- [28] L. Li, J. Zhang, Z. Peng, Y. Li, C. Gao, Y. Ji, R. Ye, N.D. Kim, Q. Zhong, Y. Yang, H. Fei, G. Ruan, J.M. Tour, *Adv. Mater.* 28 (2016) 838–845.
- [29] L. Cao, S. Yang, W. Gao, Z. Liu, Y. Gong, L. Ma, G. Shi, S. Lei, Y. Zhang, S. Zhang, R. Vajtai, P.M. Ajayan, *Small* 9 (2013) 2905–2910.
- [30] W. Si, C. Yan, Y. Chen, S. Oswald, L. Han, O.G. Schmidt, *Energy Environ. Sci.* 6 (2013) 3218–3223.
- [31] Z.S. Wu, Y.-Z. Tan, S. Zheng, S. Wang, K. Parvez, J. Qin, X. Shi, C. Sun, X. Bao, X. Feng, K. Müllen, *J. Am. Chem. Soc.* 139 (2017) 4506–4512.
- [32] J. Qin, S. Wang, F. Zhou, P. Das, S. full name check others Zheng, C. Sun, X. Bao, Z.S. Wu, *Energy Storage Mater.* 18 (2019) 397–404.
- [33] S.H. Zheng, C.J. Zhang, F. Zhou, Y. Dong, X. Shi, V. Nicolosi, Z.S. Wu, X. Bao, *J. Mater. Chem.* 7 (2019) 9478–9485.
- [34] S. Ouedi, K. Robert, D. Stievenard, T. Brousse, P. Roussel, C. Lethien, *Energy Storage Mater.* 20 (2019) 243–252.
- [35] J. Du, Y. Zhao, Z. Zhang, X. Mu, X. Jiang, B. Huang, Y. Zhang, S. Zhang, Z. Zhang, E. Xie, *J. Mater. Chem.* 7 (2019) 6220–6227.
- [36] Y. Yue, Z. Yang, N. Liu, W. Liu, H. Zhang, Y. Ma, C. Yang, J. Su, L. Li, F. Long, Z. Zou, Y. Gao, *ACS Nano* 10 (2016) 11249–11257.
- [37] S. Wang, Z.S. Wu, F. Zhou, X. Shi, S. Zheng, J. Qin, H. Xiao, C. Sun, X. Bao, *npj 2D Mater. Appl.* 2 (2018) 1–8.
- [38] X. Shi, Z.S. Wu, J. Qin, S. Zheng, S. Wang, F. Zhou, C. Sun, X. Bao, *Adv. Mater.* 29 (2017) 1703034.
- [39] S. Zheng, Z.S. Wu, S. Wang, H. Xiao, F. Zhou, C. Sun, X. Bao, H.-M. Cheng, *Energy Storage Mater.* 6 (2017) 70–97.
- [40] C. Couly, M. Alhabeab, K.L. Van Aken, N. Kurra, L. Gomes, A.M. Navarro-Suárez, B. Anasori, H.N. Alshareef, Y. Gogotsi, *Adv. Electron. Mater.* 4 (2018) 1700339.
- [41] H. Pang, Y. Zhang, W.-Y. Lai, Z. Hu, W. Huang, *Nano Energy* 15 (2015) 303–312.
- [42] P. Zhang, Y. Li, G. Wang, F. Wang, S. Yang, F. Zhu, X. Zhuang, O.G. Schmidt, X. Feng, *Adv. Mater.* 31 (2019) 1806005.
- [43] G. Sun, H. Yang, G. Zhang, J. Gao, X. Jin, Y. Zhao, L. Jiang, L. Qu, *Energy Environ. Sci.* 11 (2018) 3367–3374.
- [44] S. Zheng, J. Ma, Z.-S. Wu, F. Zhou, Y.-B. He, F. Kang, H.-M. Cheng, X. Bao, *Energy Environ. Sci.* 11 (2018) 2001–2009.
- [45] C. Shen, X. Wang, S. Li, W. Zhang, F. Kang, *J. Power Sources* 234 (2013) 302–309.
- [46] X. Shi, S. Pei, F. Zhou, W. Ren, H.-M. Cheng, Z.-S. Wu, X. Bao, *Energy Environ. Sci.* 12 (2019) 1534–1541.
- [47] S. Liu, J. Xie, H. Li, Y. Wang, H.Y. Yang, T. Zhu, S. Zhang, G. Cao, X. Zhao, *J. Mater. Chem.* 2 (2014) 18125–18131.
- [48] J. Li, S. Sollami Delekt, P. Zhang, S. Yang, M.R. Lohe, X. Zhuang, X. Feng, M. Östling, *ACS Nano* 11 (2017) 8249–8256.
- [49] C. Zhang, M.P. Kremer, A. Seral-Ascaso, S.H. Park, N. McEvoy, B. Anasori, Y. Gogotsi, V. Nicolosi, *Adv. Funct. Mater.* 28 (2018) 1705506.
- [50] C. Zhang, L. McKeon, M.P. Kremer, S.-H. Park, O. Ronan, A. Seral-Ascaso, S. Barwich, C.Ó. Coileáin, N. McEvoy, H.C. Nerl, B. Anasori, J.N. Coleman, Y. Gogotsi, V. Nicolosi, *Nat. Commun.* 10 (2019) 1795.
- [51] H. Li, S. Liu, X. Li, Z.-S. Wu, J. Liang, *Mater. Chem. Front.* 3 (2019) 626–635.
- [52] N. Kurra, B. Ahmed, Y. Gogotsi, H.N. Alshareef, *Adv. Energy Mater.* 6 (2016) 1601372.
- [53] H. Hu, T. Hua, *J. Mater. Chem.* 5 (2017) 19639–19648.
- [54] H. Zhang, Y. Cao, M.O.L. Chee, P. Dong, M. Ye, J. Shen, *Nanoscale* 11 (2019) 5807–5821.
- [55] D. Qi, Y. Liu, Z. Liu, L. Zhang, X. Chen, *Adv. Mater.* 29 (2017) 1602802.
- [56] F. Zhou, H. Huang, C. Xiao, S. Zheng, X. Shi, J. Qin, Q. Fu, X. Bao, X. Feng, K. Müllen, Z.S. Wu, *J. Am. Chem. Soc.* 140 (2018) 8198–8205.
- [57] H. Xiao, Z.S. Wu, F. Zhou, S. Zheng, D. Sui, Y. Chen, X.H. Bao, *Energy Storage Mater.* 13 (2018) 233–240.
- [58] Y. Yang, W. Gao, *Chem. Soc. Rev.* 48 (2019) 1465–1491.
- [59] J. Kim, A.S. Campbell, B.E.-F. de Ávila, J. Wang, *Nat. Biotechnol.* 37 (2019) 389–406.
- [60] M.Y. Lee, H.R. Lee, C.H. Park, S.G. Han, J.H. Oh, *Acc. Chem. Res.* 51 (2018) 2829–2838.
- [61] X. Chen, J.A. Rogers, S.P. Lacour, W. Hu, D.-H. Kim, *Chem. Soc. Rev.* 48 (2019) 1431–1433.
- [62] K. Xu, Y. Lu, K. Takei, *Adv. Mater. Technol.* 4 (2019) 1800628.
- [63] Y. Yoon, W. Cho, J. Lim, D.J. Choi, *J. Power Sources* 101 (2001) 126–129.
- [64] Y. Wang, B. Liu, Q. Li, S. Cartmell, S. Ferrara, Z.D. Deng, J. Xiao, *J. Power Sources* 286 (2015) 330–345.
- [65] H.-J. Peng, J.-Q. Huang, Q. Zhang, *Chem. Soc. Rev.* 46 (2017) 5237–5288.
- [66] Y. Shao, M.F. El-Kady, J. Sun, Y. Li, Q. Zhang, M. Zhu, H. Wang, B. Dunn, R.B. Kaner, *Chem. Rev.* 118 (2018) 9233–9280.
- [67] W. Chee, H. Lim, Z. Zainal, N. Huang, I. Harrison, Y. Andou, *J. Phys. Chem. C* 120 (2016) 4153–4172.
- [68] L. Dong, C. Xu, Y. Li, Z.-H. Huang, F. Kang, Q.-H. Yang, X. Zhao, *J. Mater. Chem.* 4 (2016) 4659–4685.
- [69] J. Qin, P. Das, S. Zheng, Z.S. Wu, *Apl. Mater.* 7 (2019), 090902.
- [70] J.-H. Sung, S.J. Kim, K.H. Lee, *J. Power Sources* 124 (2003) 343–350.
- [71] Y. Chyan, R. Ye, Y. Li, S.P. Singh, C.J. Arnsch, J.M. Tour, *ACS Nano* 2 (2018) 2176–2183.
- [72] R. Ye, D.K. James, J.M. Tour, *Acc. Chem. Res.* 51 (2018) 1609–1620.
- [73] M.G. Stanford, K. Yang, Y. Chyan, C. Kittrell, J.M. Tour, *ACS Nano* 13 (2019) 3474–3482.
- [74] R. Ye, D.K. James, J.M. Tour, *Adv. Mater.* 31 (2019) 1803621.
- [75] B. Zheng, T. Huang, L. Kou, X. Zhao, K. Gopalsamy, C. Gao, *J. Mater. Chem.* 2 (2014) 9736–9743.
- [76] D. Yu, K. Goh, Q. Zhang, L. Wei, H. Wang, W. Jiang, Y. Chen, *Adv. Mater.* 26 (2014) 6790–6797.
- [77] D. Yu, K. Goh, H. Wang, L. Wei, W. Jiang, Q. Zhang, L. Dai, Y. Chen, *Nat. Nanotechnol.* 9 (2014) 555–562.
- [78] W. Jiang, S. Zhai, Q. Qian, Y. Yuan, H.E. Karahan, L. Wei, K. Goh, A.K. Ng, J. Wei, Y. Chen, *Energy Environ. Sci.* 9 (2016) 611–622.
- [79] W. Cai, T. Lai, J. Ye, *J. Mater. Chem.* 3 (2015) 5060–5066.
- [80] N. Yu, H. Yin, W. Zhang, Y. Liu, Z. Tang, M.Q. Zhu, *Adv. Energy Mater.* 6 (2016) 1501458.
- [81] Q. Wang, X. Wang, J. Xu, X. Ouyang, X. Hou, D. Chen, R. Wang, G. Shen, *Nano Energy* 8 (2014) 44–51.

- [82] Z. Li, M. Shao, L. Zhou, R. Zhang, C. Zhang, J. Han, M. Wei, D.G. Evans, X. Duan, *Nano Energy* 20 (2016) 294–304.
- [83] H. Tang, W. Li, L. Pan, C.P. Cullen, Y. Liu, A. Pakdel, D. Long, J. Yang, N. McEvoy, G.S. Duesberg, V. Nicolosi, C. Zhang, *Adv. Sci.* 5 (2018) 1800502.
- [84] H. Tang, W. Li, L. Pan, K. Tu, F. Du, T. Qiu, J. Yang, C.P. Cullen, N. McEvoy, C. Zhang, *Adv. Funct. Mater.* 29 (2019) 1901907.
- [85] C. Zhang, Y. Ma, X. Zhang, S. Abdolhosseinzadeh, H. Sheng, W. Lan, A. Pakdel, J. Heier, F. Nüesch, *Energy Environ. Mater.* 3 (2020) 29–55.
- [86] H. Sheng, X. Zhang, Y. Ma, P. Wang, J. Zhou, Q. Su, W. Lan, E. Xie, C.J. Zhang, *ACS Appl. Mater. Interfaces* 11 (2019) 8992–9001.
- [87] M.F. El-Kady, R.B. Kaner, *Nat. Commun.* 4 (2013) 1475.
- [88] H. Xiao, Z.S. Wu, L. Chen, F. Zhou, S. Zheng, W. Ren, H.-M. Cheng, X. Bao, *ACS Nano* 11 (2017) 7284–7292.
- [89] Q. Meng, H. Wu, Y. Meng, K. Xie, Z. Wei, Z. Guo, *Adv. Mater.* 26 (2014) 4100–4106.
- [90] G. Wu, P. Tan, X. Wu, L. Peng, H. Cheng, C.F. Wang, W. Chen, Z. Yu, S. Chen, *Adv. Funct. Mater.* 27 (2017) 1702493.
- [91] Z.S. Wu, K. Parvez, X. Feng, K. Müllen, *Nat. Commun.* 4 (2013) 1–8.
- [92] Z.S. Wu, K. Parvez, S. Li, S. Yang, Z. Liu, S. Liu, X. Feng, K. Müllen, *Adv. Mater.* 27 (2015) 4054–4061.
- [93] T. Liu, S. Shi, C. Liang, S. Shen, L. Cheng, C. Wang, X. Song, S. Goel, T.E. Barnhart, W. Cai, Z. Liu, *ACS Nano* 9 (2015) 950–960.
- [94] J. Li, Q. Shi, Y. Shao, C. Hou, Y. Li, Q. Zhang, H. Wang, *Energy Storage Mater.* 16 (2019) 212–219.
- [95] J.-Q. Xie, Y.-Q. Ji, J.-H. Kang, J.-L. Sheng, D.-S. Mao, X.-Z. Fu, R. Sun, C.-P. Wong, *Energy Environ. Sci.* 12 (2019) 194–205.
- [96] Y. He, P. Zhang, F. Wang, L. Wang, Y. Su, F. Zhang, X. Zhuang, X. Feng, *Nano Energy* 60 (2019) 8–16.
- [97] X. Lu, M. Yu, G. Wang, Y. Tong, Y. Li, *Energy Environ. Sci.* 7 (2014) 2160–2181.
- [98] J. Yun, Y. Lim, H. Lee, G. Lee, H. Park, S.Y. Hong, S.W. Jin, Y.H. Lee, S.S. Lee, J.S. Ha, *Adv. Funct. Mater.* 27 (2017) 1700135.
- [99] I. Osada, H. de Vries, B. Scrosati, S. Passerini, *Angew. Chem. Int. Ed.* 55 (2016) 500–513.
- [100] D. Kim, G. Lee, D. Kim, J.S. Ha, *ACS Appl. Mater. Interfaces* 7 (2015) 4608–4615.
- [101] H. Gao, K. Lian, *RSC Adv.* 4 (2014) 33091–33113.
- [102] C. Zhong, Y. Deng, W. Hu, J. Qiao, L. Zhang, J. Zhang, *Chem. Soc. Rev.* 44 (2015) 7484–7539.
- [103] Z. Lou, G. Shen, *Adv. Sci.* 3 (2016) 1500287.
- [104] Z. Huang, J.E. Carey, M. Liu, X. Guo, E. Mazur, J.C. Campbell, *Appl. Phys. Lett.* 89 (2006), 033506.
- [105] J. Huang, Y. Wan, D. Jung, J. Norman, C. Shang, Q. Li, K.M. Lau, A.C. Gossard, J.E. Bowers, B. Chen, *ACS Photonics* 6 (2019) 1100–1105.
- [106] C. Xie, F. Yan, *Small* 13 (2017) 1701822.
- [107] Y. Yue, N. Liu, Y. Ma, S. Wang, W. Liu, C. Luo, H. Zhang, F. Cheng, J. Rao, X. Hu, J. Su, Y. Gao, *ACS Nano* 12 (2018) 4224–4232.
- [108] S. Gu, Z. Lou, L. Li, Z. Chen, X. Ma, G. Shen, *Nano Res.* 9 (2016) 424–434.
- [109] S.G. Chatterjee, S. Chatterjee, A.K. Ray, A.K. Chakraborty, *Sensor. Actuator. B Chem.* 221 (2015) 1170–1181.
- [110] E. Singh, M. Meyyappan, H.S. Nalwa, *ACS Appl. Mater. Interfaces* 9 (2017) 34544–34586.
- [111] J.W. Kim, Y. Porte, K.Y. Ko, H. Kim, J.-M. Myoung, *ACS Appl. Mater. Interfaces* 9 (2017) 32876–32886.
- [112] J. Yun, Y. Lim, G.N. Jang, D. Kim, S.-J. Lee, H. Park, S.Y. Hong, G. Lee, G. Zi, J.S. Ha, *Nano Energy* 19 (2016) 401–414.
- [113] L. Li, C. Fu, Z. Lou, S. Chen, W. Han, K. Jiang, D. Chen, G. Shen, *Nano Energy* 41 (2017) 261–268.
- [114] R. Guo, J. Chen, B. Yang, L. Liu, L. Su, B. Shen, X. Yan, *Adv. Funct. Mater.* 27 (2017) 1702394.
- [115] H. Liu, Q. Li, S. Zhang, R. Yin, X. Liu, Y. He, K. Dai, C. Shan, J. Guo, C. Liu, C. Shen, X. Wang, N. Wang, Z. Wang, R. Wei, Z. Guo, *J. Mater. Chem. C* 6 (2018) 12121–12141.
- [116] M. Amjadi, K.U. Kyung, I. Park, M. Sitti, *Adv. Funct. Mater.* 26 (2016) 1678–1698.
- [117] D. Kim, D. Kim, H. Lee, Y.R. Jeong, S.-J. Lee, G. Yang, H. Kim, G. Lee, S. Jeon, G. Zi, J. Kim, J.S. Ha, *Adv. Mater.* 28 (2016) 748–756.
- [118] J. Yun, C. Song, H. Lee, H. Park, Y.R. Jeong, J.W. Kim, S.W. Jin, S.Y. Oh, L. Sun, G. Zi, J.S. Ha, *Nano Energy* 49 (2018) 644–654.
- [119] Y. Song, H. Chen, X. Chen, H. Wu, H. Guo, X. Cheng, B. Meng, H. Zhang, *Nano Energy* 53 (2018) 189–197.
- [120] B. Schazmann, D. Morris, C. Slater, S. Beirne, C. Fay, R. Reuveny, N. Moyna, D. Diamond, *Anal. Methods* 2 (2010) 342–348.
- [121] Y. Lu, K. Jiang, D. Chen, G. Shen, *Nano Energy* 58 (2019) 624–632.
- [122] T. Wu, C.-W. Sher, Y. Lin, C.-F. Lee, S. Liang, Y. Lu, S.-W. Huang, W. Guo, H.-C. Kuo, Z. Chen, *Appl. Sci.* 8 (2018) 1557.
- [123] H. Kim, J. Yoon, G. Lee, S.-h. Paik, G. Choi, D. Kim, B.-M. Kim, G. Zi, J.S. Ha, *ACS Appl. Mater. Interfaces* 8 (2016) 16016–16025.
- [124] Y. Lim, J. Yoon, J. Yun, D. Kim, S.Y. Hong, S.-J. Lee, G. Zi, J.S. Ha, *ACS Nano* 8 (2014) 11639–11650.
- [125] D. Kim, G. Shin, Y.J. Kang, W. Kim, J.S. Ha, *ACS Nano* 7 (2013) 7975–7982.
- [126] W. Zhao, L. Wei, Q. Fu, X. Guo, *J. Power Sources* 422 (2019) 73–83.